

Social regulation of a rudimentary organ generates complex worker–caste systems in ants

Rajendhran Rajakumar^{1,2}, Sophie Koch¹, Mélanie Couture¹, Marie-Julie Favé^{1,3}, Angelica Lillico-Ouachour¹, Travis Chen¹, Giovanna De Blasis¹, Arjuna Rajakumar¹, Dominic Ouellette¹ & Ehab Abouheif^{1*}

The origin of complex worker–caste systems in ants perplexed Darwin¹ and has remained an enduring problem for evolutionary and developmental biology^{2–6}. Ants originated approximately 150 million years ago, and produce colonies with winged queen and male castes as well as a wingless worker caste⁷. In the hyperdiverse genus *Pheidole*, the wingless worker caste has evolved into two morphologically distinct subcastes—small-headed minor workers and large-headed soldiers⁸. The wings of queens and males develop from populations of cells in larvae that are called wing imaginal discs⁷. Although minor workers and soldiers are wingless, vestiges or rudiments of wing imaginal discs appear transiently during soldier development^{7,9–11}. Such rudimentary traits are phylogenetically widespread and are primarily used as evidence of common descent, yet their functional importance remains equivocal^{1,12–14}. Here we show that the growth of rudimentary wing discs is necessary for regulating allometry—disproportionate scaling—between head and body size to generate large-headed soldiers in the genus *Pheidole*. We also show that *Pheidole* colonies have evolved the capacity to socially regulate the growth of rudimentary wing discs to control worker subcaste determination, which allows these colonies to maintain the ratio of minor workers to soldiers. Finally, we provide comparative and experimental evidence that suggests that rudimentary wing discs have facilitated the parallel evolution of complex worker–caste systems across the ants. More generally, rudimentary organs may unexpectedly acquire novel regulatory functions during development to facilitate adaptive evolution.

The evolution of large-headed soldiers is thought to have promoted the adaptive radiation of *Pheidole*, which has produced approximately 1,000 species worldwide^{8,15}. *Pheidole* soldiers are larger than minor workers and their heads are disproportionately larger than their bodies, forming an allometric line that is distinct from that of minor workers (Fig. 1a–c). A developmental switch—largely controlled by nutrition⁶ and mediated by juvenile hormone¹⁶—determines whether larvae develop into minor workers or soldiers (Fig. 2a). Minor worker larvae lack wing rudiments (Fig. 2c), whereas soldier larvae have one pair of rudimentary forewing discs⁹ (Fig. 2d). In *Pheidole obtusospinosa*, which has evolved a disproportionately larger ‘supersoldier’ subcaste (Fig. 1d–f), supersoldier larvae have two pairs of large rudimentary wing discs¹⁰ (Fig. 1g–i). In addition, using Pagel’s¹⁷ phylogenetic correlation method, we found that the size of rudimentary wing discs varies discretely between worker subcastes within ant species that have independently evolved a soldier subcaste (Extended Data Fig. 1 and Extended Data Table 1). Finally, rudimentary forewing discs in *Pheidole* soldier larvae are coordinated in their growth, gene expression and apoptosis—just after larvae become determined as soldiers (Fig. 2a, red arrowhead), rudimentary forewing discs appear⁹, grow rapidly⁹ (Extended Data Fig. 2), activate expression of genes in the wing network^{7,10} and are finally eliminated by apoptosis¹¹. These findings raise the possibility that rudimentary wing discs have a functional role in the development of soldiers.

We tested this possibility in *Pheidole hyatti* by targeting *vestigial* (*vg*), which in *Drosophila* is a selector gene that coordinates growth and patterning of wing imaginal discs and is necessary and sufficient for wing development^{18–20}. Spatial expression of *vg* is similar in *P. hyatti* and *Drosophila*—in embryos *vg* is expressed in wing primordia and the ventral nerve cord, but in larvae *vg* expression could be detected only in the wing discs of winged castes and in the rudimentary forewing discs of soldiers (Fig. 2b–d and Extended Data Fig. 3a–o). We therefore used RNA-mediated interference (RNAi) to knockdown *vg* expression in soldier-destined larvae (Fig. 2a, red arrowhead). Compared to controls, *vg* RNAi significantly reduces the size of rudimentary forewing discs (Fig. 2e–g) and, as in *Drosophila* wing discs, perturbing *vg* expression induces apoptosis (Extended Data Fig. 4). We discovered that reducing the size of rudimentary forewing discs affects the adult phenotype: it significantly reduces the head/body ratio and changes the head-to-body slope such that head size is reduced more than body size, relative to controls (Fig. 2h, i and Extended Data Fig. 5a–f). These ants vary widely in head and body size, from being as small as minor workers to being as large as soldiers—some ants are intermediate in size, which are variants that do not exist in nature (Fig. 2i and Extended Data Fig. 5g–l). Finally, *vg* has also been shown to be expressed outside of wing discs in *Drosophila* larvae²¹. To confirm that *vg* RNAi changes head-to-body scaling by specifically reducing the size of rudimentary forewing discs, we electro-surgically ablated the left rudimentary forewing disc in soldier-destined larvae; as a control, we ablated the third leg disc on the left side (Fig. 2a, red arrowhead and Extended Data Fig. 5m–q). These ablations produced results similar to *vg* RNAi (Fig. 2j, k and Extended Data Fig. 5r–t). Together, these experiments show that rudimentary forewing discs are necessary to regulate the size and disproportionate head-to-body scaling that generates large-headed soldiers.

Minor worker larvae lack rudimentary wing discs and do not express *vg* in any other imaginal discs (Fig. 2c and Extended Data Fig. 3e, h, k, n). However, we found low levels of expression of *vg* outside of imaginal discs in minor worker larvae (Extended Data Fig. 3p). To test whether this expression influences head-to-body scaling, we treated bipotential larvae (Fig. 2a, orange arrowhead)—of which 90–95% develop into minor workers, and 5–10% into soldiers¹⁶—with *vg* RNAi. The bipotential larvae treated with *vg* RNAi that became minor workers did not show significant differences in size, head/body ratio, slope or intercept compared to controls (Extended Data Fig. 6a, b, e, g–i), whereas the few that developed into soldier-destined larvae became intermediates (Extended Data Fig. 6c, d, f). Therefore, expression of *vg* outside of imaginal discs does not influence size or head-to-body scaling in the minor-worker subcaste. We then investigated whether wing discs in winged castes regulate head-to-body scaling. Relative to controls, we found that in larvae destined to become males (Fig. 2a, green arrowhead) *vg* RNAi causes defects in patterning and growth of adult fore- and hindwings (Extended Data Fig. 6j–l), but has no significant effect on size, head/body ratio, slope or intercept (Extended Data Fig. 6m–p). Therefore, wing discs in male larvae produce wings

¹Department of Biology, McGill University, Montreal, Quebec, Canada. ²Present address: Department of Genetics, Harvard Medical School, Boston, MA, USA. ³Present address: Ontario Institute for Cancer Research, Toronto, Ontario, Canada. *e-mail: ehab.abouheif@mcgill.ca

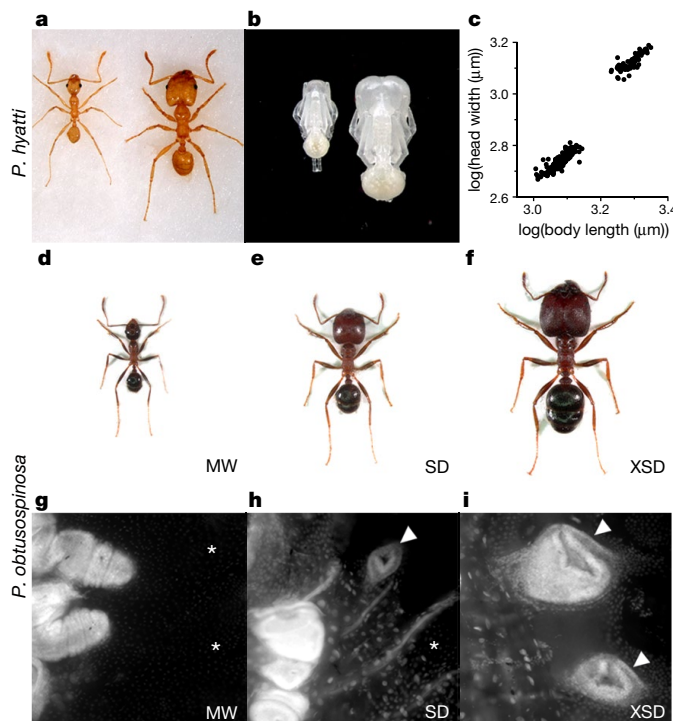


Fig. 1 | Head-to-body allometry and rudimentary wing discs of *Pheidole* worker subcastes. **a**, *P. hyatti* minor worker adult (left) and soldier adult (right). **b**, *P. hyatti* minor worker pupa (left) and soldier pupa (right). **c**, log–log plot of head-to-body allometry of wild-type minor workers ($n = 155$) and soldiers ($n = 80$) (x and y axes in μm). **d–i**, Comparing *P. obtusospinosa* worker subcastes and rudimentary wing discs (comparisons to scale): minor worker (MW, **d**, **g**), soldier (SD, **e**, **h**) and supersoldier (XSD, **f**, **i**). Arrowheads indicate rudimentary wing discs; asterisk indicates absence of a rudimentary wing disc.

but do not regulate size or head-to-body scaling. These results show that, within the wingless female worker caste, rudimentary forewing discs regulate the size and disproportionate head-to-body scaling that is specific to the soldier subcaste.

Pheidole colonies dynamically maintain a ratio of soldiers (5–10%) to minor workers (90–95%): soldiers use their large heads for defence and food processing, and minor workers forage and nurse young^{8,22–25}. This ratio is maintained through the balance of two types of social regulation: (1) the activation of soldier development by minor workers through nutrition⁶, which is mediated by juvenile hormone¹⁶; and (2) the suppression of soldier development through an inhibitory pheromone when the number of soldiers increases to above 5–10%^{23,24}. This pheromone is contact-based and is thought to be composed of cuticular hydrocarbons^{23,24,26}. Because juvenile hormone induces rudimentary forewing disc growth in *P. hyatti*¹⁰, we investigated whether their growth is also influenced by the inhibitory pheromone. We therefore raised soldier-destined larvae (Fig. 2a, red arrowhead) with either 100% soldiers (high inhibition) or 100% minor workers (no inhibition, as a control). We discovered that raising soldier-destined larvae with 100% soldiers significantly reduces the size of rudimentary forewing discs, relative to controls (Fig. 3a–c). This produced ants with a significantly reduced head/body ratio and changes the head-to-body slope such that head size is reduced more than body size, relative to controls (Fig. 3d, e and Extended Data Fig. 7a–f). These ants vary widely in size, ranging from minor workers to soldiers, and include intermediates (Fig. 3e and Extended Data Fig. 7g–k). Finally, to rule out the possibility that these results are caused by any potential differences in the rearing environments of minor workers and soldiers, we treated soldier-destined larvae with cuticular hydrocarbons extracted from soldiers and compared them to solvent-only controls under identical rearing conditions (100% minor workers). This produced

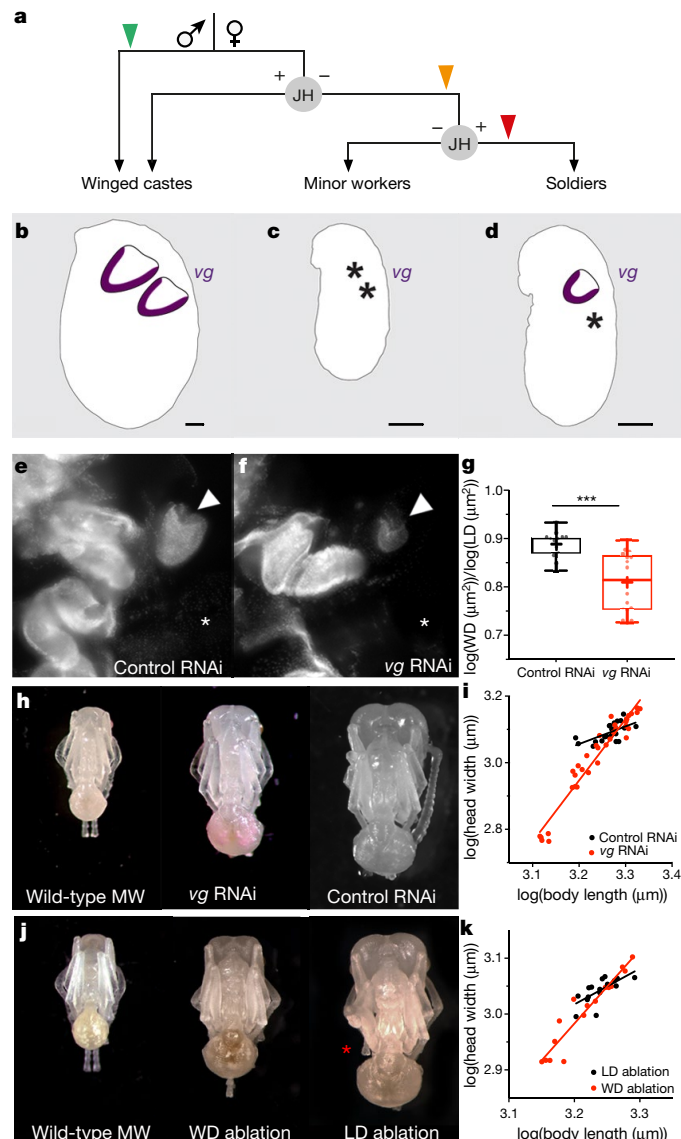


Fig. 2 | Rudimentary forewing discs regulate size and disproportionate head-to-body scaling of soldiers. **a**, Caste determination in *Pheidole* at three developmental switch points produces: winged males, wingless queens, wingless minor workers and wingless soldiers. Points of experimental manipulation are indicated by coloured arrowheads: red, soldier-destined larvae; orange, bipotential larvae; green, male-destined larvae. JH, juvenile hormone. **b–d**, *vg* expression (purple) in larval wing discs of males or queens (**b**), minor workers (**c**) and soldiers (**d**). Black asterisk, absence of rudimentary wing disc. Scale bars, relative scale. **e–f**, Rudimentary forewing discs after *yfp* RNAi (control RNAi) (**e**) or *vg* RNAi (**f**). Rudimentary wing disc presence (white arrowheads) or absence (white asterisks). **g**, Comparing ratio of log(rudimentary forewing disc area (μm^2)) to log(leg disc area (μm^2)) ($\log(\text{WD} (\mu\text{m}^2))/\log(\text{LD} (\mu\text{m}^2))$) between control RNAi ($n = 13$) and *vg* RNAi ($n = 16$). The box plot shows mean (+), interquartile range (bars) and minimum to maximum values (whiskers); all points represent individual ants. Two-tailed Mann–Whitney *U*-test, $U = 24$, *** $P = 0.0002$. **h**, Wild-type minor worker and representative individuals treated with control RNAi or *vg* RNAi. **i**, Comparing slopes of control RNAi ($n = 23$) and *vg* RNAi ($n = 35$); analysis of covariance (ANCOVA), $F = 38.1$, degrees of freedom (d.f.) = 54, $P < 0.0001$. Experiments were repeated at least three times. **j**, Wild-type minor worker and treated individuals with either rudimentary forewing disc or leg disc ablated. Red asterisk, ablated leg. **k**, Comparing slopes of leg disc ($n = 16$) and rudimentary forewing disc ablations ($n = 16$); ANCOVA, $F = 8.74$, d.f. = 28, $P = 0.0063$. Image comparisons are to scale. Experiments were repeated at least twice. All regressions are x axis ($\log(\text{body length} (\mu\text{m}))$) versus y axis ($\log(\text{head width} (\mu\text{m}))$).

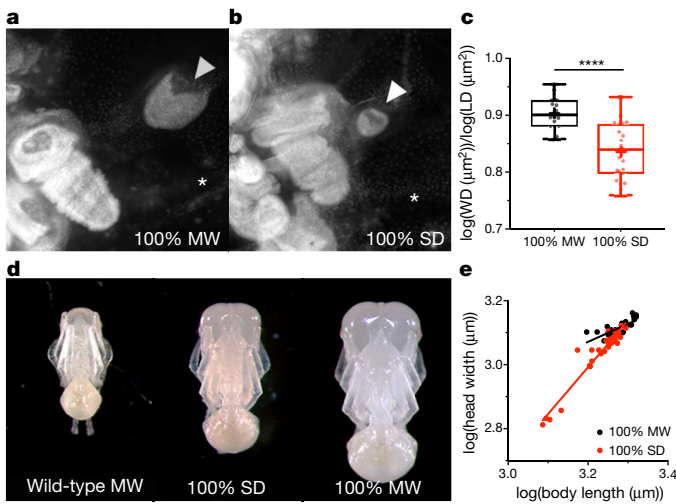


Fig. 3 | Social inhibition regulates size and disproportionate head-to-body scaling by suppressing growth of rudimentary forewing discs. Manipulations are on soldier-destined larvae. Rudimentary wing disc presence (arrowheads) or absence (asterisks). **a, b.**, Comparing rudimentary wing disc size after no inhibition (100% minor workers) (**a**) and high inhibition (100% soldiers) (**b**). **c.**, Comparing ratios of $\log(\text{rudimentary forewing disc area } (\mu\text{m}^2))$ to $\log(\text{leg disc area } (\mu\text{m}^2))$ between 100% minor workers ($n = 18$) and 100% soldiers ($n = 23$). The box plot shows mean (+), interquartile range (bars) and minimum to maximum values (whiskers); all points represent individual ants. Two-tailed unequal variance t -test, $t = 5.77$, $\text{d.f.} = 36.13$, $****P < 0.0001$. **d.**, Wild-type minor worker and representative individuals raised by 100% minor workers or 100% soldiers. **e.**, Comparing slopes of 100% minor workers ($n = 24$) and 100% soldiers ($n = 35$); ANCOVA, $F = 36.55$, $\text{d.f.} = 55$, $P < 0.0001$; x axis ($\log(\text{body length } (\mu\text{m}))$) versus y axis ($\log(\text{head width } (\mu\text{m}))$). Image comparisons are to scale. Experiments were repeated at least three times.

results similar to the larvae raised entirely by soldiers (Extended Data Fig. 7l–p). Taken together, the soldier inhibitory pheromone regulates size and disproportionate head-to-body scaling by suppressing growth of rudimentary forewing discs.

We next investigated whether rudimentary forewing discs mediate the interaction between the inhibitory pheromone and juvenile hormone to regulate size, head-to-body scaling and worker subcaste determination. Previous work²⁴ has demonstrated that the inhibitory pheromone acts downstream of juvenile hormone and can inhibit activation of soldier development—bipotential larvae treated with juvenile hormone and raised entirely by soldiers can block soldier development, which results in the production of large minor workers²⁴. In *P. hyatti*, we found that these large minor workers develop from larvae that lack rudimentary forewing discs and are proportionally larger; although the intercept is significantly different relative to controls, the head-to-body slope is not (Extended Data Fig. 8i–l). Conversely, treating bipotential larvae with juvenile hormone but without inhibitory pheromone (100% minor workers) produced soldiers that crossed the juvenile-hormone threshold, as well as large minor workers that did not (Extended Data Fig. 8a–d). These large minor workers, which develop from larvae with rudimentary forewing discs that prematurely stop growing, are disproportionately larger; the head-to-body slope is significantly different compared to controls (Extended Data Fig. 8e–h). These results show that: (1) blocking growth of rudimentary forewing discs with inhibitory pheromone blocks the disproportionate head-to-body scaling that is induced by juvenile hormone; and (2) juvenile hormone regulates size and proportional head-to-body scaling independently of rudimentary forewing discs (Fig. 4a). Finally, to determine the role of inhibitory pheromone independent of rudimentary forewing discs, we exposed bipotential larvae to inhibitory pheromone (100% soldiers) without treatment with juvenile hormone. The minor workers that

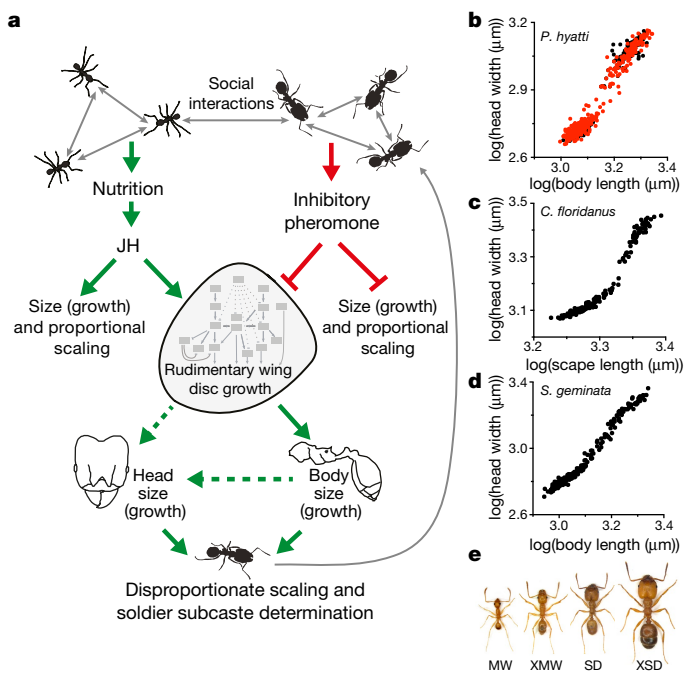


Fig. 4 | The role of rudimentary wing discs in the social regulation, development and evolution of complex worker-caste systems in ants. **a.**, Interactions (arrows and lines) may be direct or indirect. Green arrows, activation; dashed green arrows, potential pathways to disproportionate scaling; red arrows and lines, inhibition; grey arrows, social interactions; grey circle, rudimentary forewing discs; grey boxes, wing gene network. **b.**, Experimental manipulations (red) and controls (black) in *P. hyatti*. **c.**, Wild-type *C. floridanus* workers²⁹ ($n = 179$). **d.**, Wild-type *S. geminata* workers³⁰ ($n = 239$). Plots in **b–d** show $\log(\text{body length } (\mu\text{m}))$ or $\log(\text{scape length } (\mu\text{m}))$ on the x axis, versus $\log(\text{head width } (\mu\text{m}))$ on the y axis. **e.**, Comparison, to scale, of wild-type minor worker, large minor worker anomaly (XMW), wild-type soldier and supersoldier-like anomaly (XSD).

result develop from larvae that lack rudimentary forewing discs and are proportionally smaller; although the intercept is significantly different, the head-to-body slope is not (Extended Data Fig. 8m–p). Taken together, we show that juvenile hormone and the inhibitory pheromone regulate size and proportional head-to-body scaling independently of rudimentary forewing discs (Fig. 4a). By contrast, juvenile hormone and the inhibitory pheromone regulate size, disproportionate head-to-body scaling, and soldier subcaste determination, by directly or indirectly influencing the growth of rudimentary forewing discs (Fig. 4a).

Multiple molecular mechanisms may underlie the function of rudimentary wing discs. Organs, including wing imaginal discs in insects, communicate through conserved signalling pathways to coordinate development²⁷. In flies, butterflies and beetles, eliminating or reducing the growth of one imaginal disc either increases the size of others owing to resource competition, or has no adult phenotypic effect owing to homeostasis²⁸. By contrast, we show that eliminating or reducing the growth of a rudimentary wing disc decreases the head/body ratio. The rudimentary forewing discs may increase head growth secondarily, through their influence on body growth. Alternatively, because rudimentary forewing discs increase head size more than body size, they may increase head and body growth independently of each other (Fig. 4a, dashed lines). Therefore, this ancient communication system may have been exploited and modified in *Pheidole*, enabling rudimentary wing discs to regulate head-to-body allometry at the level of the individual and the subcaste ratio at the colony level in response to environmental variation and challenges^{22–25} (Fig. 4a).

Wilson proposed³ that worker-caste systems in ants—which range from being monomorphic to completely dimorphic—have evolved through a series of developmental transitions in allometry. Our experimental manipulations of the growth of rudimentary forewing discs

produced intermediate variants that fill the empty phenotypic space between minor workers and soldiers (compare Fig. 1c to Fig. 4b). These manipulations transform *P. hyatti* from a completely dimorphic worker-caste system to a sigmoid-like allometry, which mimics the worker-caste system of other species such as *Camponotus floridanus*²⁹ or *Solenopsis geminata*³⁰ (Fig. 4b–d). Furthermore, we discovered rare and anomalously large minor workers in a wild *P. hyatti* colony (Fig. 4e), which suggests that the intermediates we produced experimentally can appear in nature but that selection for a robust juvenile-hormone-mediated threshold between minor workers and soldiers may limit their production. We also discovered rare supersoldier-like anomalies in a wild *P. hyatti* colony (Fig. 4e). Because an ancestral developmental potential to produce supersoldiers has been retained across *Pheidole*, such anomalies can be experimentally induced with juvenile hormone¹⁰. Supersoldier anomalies develop from larvae with two pairs of rudimentary wing discs¹⁰, which mimics the development of supersoldiers in *P. obtusospinosa*¹⁰ (Fig. 1f, i). These findings show that rudimentary wing discs store an ancestral developmental potential that—when released—produces allometric variation that mimics the worker-caste systems of other species (Fig. 4b–d). This potential may facilitate ‘Wilson’s transitions’³ between different complex worker-caste systems, and their parallel evolution across the ants (Extended Data Fig. 1).

The transient appearance of rudimentary organs is a general feature of organismal development, and is primarily used to infer common ancestry^{1,12–14}. Although the functional importance of rudimentary organs is enigmatic^{1,12–14}, we show that rudimentary wing discs have a major regulatory role during ant development and evolution. We propose that rudimentary organs may generally evolve key regulatory functions and, through their capacity to store and release ancestral developmental potential, may be an underappreciated source of variation that fuels adaptive evolution.

Online content

Any methods, additional references, Nature Research reporting summaries, source data, statements of data availability and associated accession codes are available at <https://doi.org/10.1038/s41586-018-0613-1>.

Received: 7 December 2017; Accepted: 22 August 2018;

Published online 10 October 2018.

1. Darwin, C. *On the Origin of Species* (John Murray, London, 1859).
2. Huxley, J. *Problems of Relative Growth* (Methuen, London, 1932).
3. Wilson, E. O. The origin and evolution of polymorphism in ants. *Q. Rev. Biol.* **28**, 136–156 (1953).
4. Wheeler, D. E. The developmental basis of worker caste polymorphisms in ants. *Am. Nat.* **138**, 1218–1238 (1991).
5. Molet, M., Wheeler, D. E. & Peeters, C. Evolution of novel mosaic castes in ants: modularity, phenotypic plasticity, and colonial buffering. *Am. Nat.* **180**, 328–341 (2012).
6. Metzl, C., Wheeler, D. E. & Abouheif, E. Wilhelm Goetsch (1887–1960): pioneering studies on the development and evolution of the soldier caste in social insects. *Myrmecol. News* **26**, 81–96 (2018).
7. Abouheif, E. & Wray, G. A. Evolution of the gene network underlying wing polyphenism in ants. *Science* **297**, 249–252 (2002).
8. Wilson, E. O. *Pheidole in the New World* (Harvard Univ. Press, Cambridge, 2003).
9. Wheeler, D. E. & Nijhout, H. F. Imaginal wing discs in larvae of the soldier caste of *Pheidole bicarinata vinelandica* Forel (Hymenoptera: Formicidae). *Int. J. Insect Morphol. Embryol.* **10**, 131–139 (1981).
10. Rajakumar, R. et al. Ancestral developmental potential facilitates parallel evolution in ants. *Science* **335**, 79–82 (2012).
11. Sameshima, S.-Y., Miura, T. & Matsumoto, T. Wing disc development during caste differentiation in the ant *Pheidole megacephala* (Hymenoptera: Formicidae). *Evol. Dev.* **6**, 336–341 (2004).
12. Gould, S. J. *Ontogeny and Phylogeny* (Belknap, Cambridge, 1977).
13. Mayr, E. Recapitulation reinterpreted: the somatic program. *Q. Rev. Biol.* **69**, 223–232 (1994).

14. Hall, B. K. Descent with modification: the unity underlying homology and homoplasy as seen through an analysis of development and evolution. *Biol. Rev. Camb. Philos. Soc.* **78**, 409–433 (2003).
15. Economo, E. P. et al. Global phylogenetic structure of the hyperdiverse ant genus *Pheidole* reveals the repeated evolution of macroecological patterns. *Proc. R. Soc. Lond. B* **282**, 20141416 (2015).
16. Wheeler, D. E. & Nijhout, H. F. Soldier determination in ants: new role for juvenile hormone. *Science* **213**, 361–363 (1981).
17. Pagel, M. Detecting correlated evolution on phylogenies: a general method for the comparative analysis of discrete characters. *Proc. R. Soc. Lond. B* **255**, 37–45 (1994).
18. Williams, J. A., Bell, J. B. & Carroll, S. B. Control of *Drosophila* wing and haltere development by the nuclear vestigial gene product. *Genes Dev.* **5**, 2481–2495 (1991).
19. Van de Bor, V., Delanoue, R., Cossard, R. & Silber, J. Truncated products of the *vestigial* proliferation gene induce apoptosis. *Cell Death Differ.* **6**, 557–564 (1999).
20. Kim, J. et al. Integration of positional signals and regulation of wing formation and identity by *Drosophila* *vestigial* gene. *Nature* **382**, 133–138 (1996).
21. Zider, A., Flagiello, D., Frouin, I. & Silber, J. *Vestigial* gene expression in *Drosophila melanogaster* is modulated by the dTMP pool. *Mol. Gen. Genet.* **251**, 91–98 (1996).
22. Yang, A. S., Martin, C. H. & Nijhout, H. F. Geographic variation of caste structure among ant populations. *Curr. Biol.* **14**, 514–519 (2004).
23. Lillico-Ouachour, A. & Abouheif, E. Regulation, development, and evolution of caste ratios in the hyperdiverse ant genus *Pheidole*. *Curr. Opin. Insect Sci.* **19**, 43–51 (2017).
24. Wheeler, D. E. & Nijhout, H. F. Soldier determination in *Pheidole bicarinata*: inhibition by adult soldiers. *J. Insect Physiol.* **30**, 127–135 (1984).
25. Passera, L., Roncin, E., Kaufmann, B. & Keller, L. Increased soldier production in ant colonies exposed to intraspecific competition. *Nature* **379**, 630–631 (1996).
26. Lillico-Ouachour, A. *The Behavioural, Chemical, and Morphological Basis of Caste Regulation in the Worker Caste of Ants*. MSc thesis, McGill Univ. (2017).
27. Droujinine, I. A. & Perrimon, N. Interorgan communication pathways in physiology: focus on *Drosophila*. *Annu. Rev. Genet.* **50**, 539–570 (2016).
28. Shingleton, A. W. & Franklin, W. A. The (ongoing) problem of relative growth. *Curr. Opin. Insect Sci.* **25**, 9–19 (2018).
29. Alvarado, S., Rajakumar, R., Abouheif, E. & Szyf, M. Epigenetic variation in the *Egr1* gene generates quantitative variation in a complex trait in ants. *Nat. Commun.* **6**, 6513 (2015).
30. Tschinkel, W. R. The morphometry of *Solenopsis* fire ants. *PLoS ONE* **8**, e79559 (2013).

Acknowledgements We thank R. Johnson, K. Haight, A. Wild, L. Davis, R. Sanwald and A. Nispel for help collecting ants; J. Liebig for help with cuticular hydrocarbon experiments; T. Oakley and P. Ward for help with phylogenetic analyses; and Y. Tomoyasu, I. Ruvinsky, B. Hall, D. E. Wheeler, D. Schoen, A. Shingleton, V. Callier, G. Wray, S. C. Weber, members of the Abouheif Laboratory, M. J. West-Eberhard and E. O. Wilson for comments on the manuscript. We thank the McGill University Advanced Biolumaging Facility for imaging support. This work was supported by KLI fellowships (Austria) to R.R. and E.A., and NSERC Discovery Grant and Steacie Fellowship (Canada) and Guggenheim Fellowship (USA) to E.A.

Author contributions E.A. and R.R. conceived the project and designed experiments; E.A., R.R., A.R. and S.K. collected ants; R.R., S.K., M.C. and A.R. performed *in situ* hybridization and immunohistochemistry; R.R., M.-J.F., M.C., S.K. and T.C. performed RNAi; S.K. performed ablations; R.R., G.D.B., A.L.-O., M.C. and T.C. performed pheromone experiments; R.R., M.C., M.-J.F., A.L.-O., S.K., G.D.B. and T.C. performed hormone experiments; T.C. and R.R. performed semi-quantitative PCR; E.A. performed phylogenetic analyses; and D.O. mounted adult specimens. E.A. and R.R. wrote the manuscript with input from co-authors.

Competing interests The authors declare no competing interests.

Additional information

Extended data is available for this paper at <https://doi.org/10.1038/s41586-018-0613-1>.

Supplementary information is available for this paper at <https://doi.org/10.1038/s41586-018-0613-1>.

Reprints and permissions information is available at <http://www.nature.com/reprints>.

Correspondence and requests for materials should be addressed to E.A.

Publisher's note: Springer Nature remains neutral with regard to jurisdictional claims in published maps and institutional affiliations.

METHODS

Animal collection and culturing. Colonies of *P. hyatti* and *P. obtusospinosa* were collected in the southwest of Arizona, USA. *C. floridanus* colonies were collected as newly mated queens in Tallahassee, Florida, USA. *Monomorium trageri* colonies and *S. geminata* larvae were collected in Gainesville, Florida, USA. All colonies and experimental replicates were kept at 27 °C with 60% humidity and a 12:12-light:dark cycle. They were kept in fluon-coated plastic boxes with cotton-constrained glass water tubes as well as sugar water tubes. They were fed mealworms and Bhatkar–Whitcomb diet³¹. Holes were inserted in the lids of the boxes and lined with mesh to allow better air exchange. All experiments were performed in accordance with invertebrate care guidelines and regulations.

Testing for phylogenetic correlation. Pagel's¹⁷ maximum likelihood based phylogenetic correlation test, as implemented in Mesquite 3.5³², was used to test for a phylogenetic correlation between the evolution of inter-subcaste variation in size of rudimentary wing discs and evolution of a soldier subcaste. One hundred extra iterations were used to set the intensity of the likelihood search. Pagel's¹⁷ method first calculates the log-likelihood that the presence of inter-subcaste variation in the size of rudimentary wing discs and the presence of soldier subcastes evolved independently of each other along the phylogeny, and then calculates the log-likelihood that both traits evolved in a correlated manner along the phylogeny. It then uses a likelihood ratio test statistic (1,000 simulations of the data were used) to determine which of these two models best fits the data. For data on the size of rudimentary wing discs and soldier subcastes, all available comparative data from the literature and from the present study were collected, resulting in data points for 21 species across 10 ant genera (Extended Data Fig. 1 and Extended Data Table 1). Phylogenetic relationships and branch-length information were obtained for all 21 species (Extended Data Fig. 1a) from previous publications^{33–40}, and provide formal phylogenetic evidence that a soldier subcaste has evolved several times independently across the ants. For each species, the presence of inter-subcaste variation in size of rudimentary wing discs was coded as a '1' if rudimentary wing discs were discretely larger in the soldier subcaste compared to the minor-worker subcaste (Extended Data Table 1). Inter-subcaste variation in size of rudimentary wing discs was coded as '0' if inter-subcaste variation was absent and larvae in the colony had similar sizes of rudimentary wing discs (Extended Data Table 1). For each species, the presence of a soldier subcaste was coded as '1' if it was demonstrated by previous studies (Extended Data Table 1). The absence of a soldier subcaste was coded as '0' if it was demonstrated by previous studies (Extended Data Table 1).

Isolation of vestigial homologues. Forward: 5'-TATCCTTACCTKTAYC ARACCC-3' and reverse: 5'-GCTGACTATTCCAAAAGGARGG-3' degenerate primers were designed based on a *vestigial* sequence alignment of *Tribolium castaneum* (XM_008201106), *Apis mellifera* (XM_001122002.4) and several ant species obtained from the Ant Genome Portal database (http://hymenopterogenome.org/ant_genomes/). *P. hyatti* RNA was isolated using TRIzol (Invitrogen) from a pool of embryos and larvae of different developmental stages. RNA was then reverse-transcribed to synthesize a cDNA library. PCR amplicons were ligated into the pGEM-T easy vector (Promega) and subsequently sequenced (MH683613) using Sanger sequencing at the Genome Quebec Innovation Centre at McGill University. To determine whether these *vestigial* sequences—including the TONDU/vestigial domain—are conserved, amino acid alignment was performed using Geneious Alignment on Geneious (R8), followed by manual alignment (Supplementary Fig. 2).

Whole-mount in situ hybridization. Terminal stage embryos and larvae were fixed and processed as previously described^{7,41–43}. Using a Zeiss Discovery V12 stereomicroscope, fixed samples were then dissected to remove the gut and fat tissue to facilitate probe access to imaginal tissues. Digoxigenin-labelled riboprobes (Roche Diagnostics Canada) for *vestigial* and *wingless*⁷ were then synthesized from the cloned *P. hyatti* fragments and subsequently used for spatial gene expression profiling in embryos⁴² and larvae⁴⁴. Reproductive, soldier and minor worker larvae were pooled during *in situ* hybridization.

Semi-quantitative reverse-transcription PCR of vestigial transcripts in *P. hyatti*. *vestigial* expression in wild-type terminal *P. hyatti* larvae was determined through the detection of *vestigial* transcripts using semi-quantitative PCR with reverse transcription (Extended Data Fig. 3 and Supplementary Fig. 1). The housekeeping gene *Elongation factor 1 alpha* (*EF1a*) was used as our reference gene because it has previously been validated as a reference gene for quantitative PCR with reverse transcription in social insects⁴⁵. Therefore, *EF1a* was first cloned and sequenced (MH683615) from a *P. hyatti* cDNA library using the following degenerate primers: forward 5'-GATTCYGGCAAGTCGACCA-3' and reverse 5'-GGAACCTTGGAAAGCCTCAAC-3'. The PCR product was sequenced using Sanger sequencing at the Genome Quebec Innovation Centre at McGill University. To extract RNA, three minor worker larvae and three soldier larvae at the terminal stage were collected from a laboratory colony and total RNA was extracted from minor workers and soldiers separately. The tissue was disrupted using a TissueLyser (Qiagen) bead mill and RNA was extracted

using the TRIzol (Invitrogen) RNA extraction protocol⁴⁶, and then purified using the RNeasy Plus Kit (Qiagen). Minor worker and soldier RNA was treated with DNase I (Invitrogen) to remove genomic DNA before being reverse transcribed into cDNA using the Superscript III First-Strand Synthesis System (Invitrogen). The concentrations of total RNA and total cDNA were normalized between minor workers and soldiers before cDNA synthesis and PCR, respectively. The two cDNA libraries were used as PCR templates for the semi-quantitative PCR with reverse transcription of *vestigial* and *EF1a*. The *P. hyatti vestigial* PCR primers used were: forward 5'-TCCTTACCTGTATCAGACCCATC-3' and reverse 5'-TGTCGATCTGCGTGTCAAAGATC-3', and the *P. hyatti EF1a* PCR primers used were: forward 5'-TCAGGACGTGTACAAGATC-3' and reverse 5'-CAATGACCTGTGCAGTAAAG-3'. The PCR was performed using an annealing temperature of 56 °C with 31 thermocycles and four serial dilutions of the two cDNA libraries (500 ng, 250 ng, 125 ng and 62.5 ng) were used for the semi-quantitative PCR with reverse transcription. A no-template water control was used to confirm absence of contamination.

Phospho-histone H3 (PH3) assay. To assay for proliferation, rudimentary wing imaginal discs from soldier-destined larvae measuring 2.2 mm, 2.5 mm and 2.7 mm in size were fixed and dissected (as described in 'Whole-mount *in situ* hybridization'), and then immunohistochemistry against PH3 was performed as previously described⁴⁷. Mouse monoclonal anti-PH3 (PH3 Ser10, Cell Signaling Technology, 9706S) primary antibody was used at a 1:25 dilution and the secondary antibody, goat anti-mouse Alexa 555 (AbCam, AB150114) was used at a 1:500 dilution. Samples were counter-stained with DAPI.

RNAi. To functionally knock down *vestigial*, *vg* double-stranded RNA (dsRNA) was synthesized from the same plasmid from which the *vg* *in situ* riboprobe was synthesized. The fragment (not including primer regions) was 631 bp, which is of a size range that is known to be highly efficient in targeting imaginal discs of other insects⁴⁸. T7-flanked (uppercase) *vg* forward 5'-TAATACGACTCACTATAGGtAtacccatctgtaccagaccc-3' and reverse 5'-TAATACGACTCACTATAGGGctgactattccaaaaggaggg-3' primers were used to amplify a template for T7 RNA polymerase to synthesize the dsRNA^{49,50}. dsRNA was then purified with the Qiagen RNAeasy purification kit followed by ethanol precipitation and eluted in Spradling injection buffer⁵¹ to a concentration of 3.5 mg/ml.

Size-matched soldier-destined larvae were then injected with *vestigial* dsRNA or with *yfp* dsRNA or injection buffer as a control. Soldier-destined larvae can be defined as larvae that ranged from 2.2 to 2.75 mm, and these larvae possess a characteristic brown gut²⁹. Larvae at this stage were specifically injected, because this is when the rudimentary forewing imaginal discs appear and begin to grow in *Pheidole*¹⁰ and at this stage *vg* expression in the wing discs of *Drosophila* is required¹⁸. To test whether *vg* RNAi affects head-to-body scaling independently of the wing disc, size-matched bipotential larvae—which are defined as ranging from 1.0 to 1.6 mm¹⁰—were injected with *vg* dsRNA because 95% of bipotential larvae develop into minor worker larvae that lack rudimentary wing discs. Finally, to determine the effect of *vg* RNAi on wing imaginal discs that develop into functional wings, size-matched male-destined larvae were injected, and wing phenotypes were examined and head width and body size (Weber's length) were measured.

To inject soldier-destined, bipotential and male larvae, the larvae were placed onto two-sided tape on a microscope slide and stabilized along a glass capillary tube. Needles were made using a Sutter Instrument needle puller (Model P-97) and inserted onto a Narishige microinjection apparatus attached to a Zeiss Discovery V8 dissection microscope fitted with a custom-made *x-y* movable platform. Microinjection flow pressure was controlled using a Cell Tram Vario 5176 (Eppendorf). Larvae were injected, while on their dorsum, through their lateral side at the midline of the antero-posterior axis. After the injection, larvae were placed in replicates containing adult minor workers to care for them (in a 2:1 adult:larva ratio) until they were either fixed before pupation and DAPI-stained for imaginal disc imaging and measurements, left to metamorphose into pupae for pupal imaging and measurements or—in the case of males—left to become adults for measurements.

Efficiency and specificity of *vg* RNAi. Semi-quantitative reverse-transcription PCR was performed on terminal *P. hyatti* soldier larvae after injection with *vg* RNAi or *yfp* RNAi to confirm knockdown of *vg* transcripts (Extended Data Fig. 4 and Supplementary Fig. 1). RNA was extracted from terminal soldier larvae 48 h post-injection and cDNA libraries were synthesized and standardized as described above. *NADH* (*NADH-ubiquinone oxidoreductase subunit 8*) was used as a reference gene as it has previously been validated as a reference gene for quantitative PCR in ants⁵². Therefore, *NADH* was first cloned and sequenced (MH683614) from a *P. hyatti* cDNA library using the following degenerate primers: forward 5'-GGGBCCTTACAGATAATTGCRC-3' and reverse 5'-ATTCAAGTTRGGACCCTCA-3'. The two cDNA libraries (*vg* RNAi and *yfp* RNAi) were used as PCR templates for the semi-quantitative reverse-transcription PCR of *vestigial* and *NADH*. The *NADH* *P. hyatti*

primers were: forward 5'-GGGAGAGCATGCGTTAAGAA-3' and reverse 5'-TAGCCTGTGCAGGACAAATC-3'. The *vestigial* primers targeting outside the dsRNA fragment were: forward 5'-CATTACCCACAGTACCATCACA-3' and reverse 5'-CAGCAGAAGGCCACTGTAG-3'. The PCR was performed using an annealing temperature of 60°C with 35 thermocycles and four serial dilutions of the two cDNA libraries were used as template. A no-template water control was used to confirm absence of contamination.

Finally, the TUNEL (TdT-mediated dUTP nick end labelling) assay was used to validate the specificity of *vg* RNAi because perturbation of *vg* expression is known to induce apoptosis in *Drosophila* wing imaginal discs¹⁹. Apoptotic cell death was assayed using the In Situ Cell Death Detection Kit, AP (Roche Diagnostics). The protocol was carried out as in a previous publication⁵³, with a modification of the proteinase K step to 5 min (50 µg/ml).

Ablations. The ablation protocol was modified from a previous publication⁵⁴. Soldier-destined larvae were collected, as described in 'RNAi'. Leg and rudimentary wing disc ablations were done using a Hyfrecator 2000 electrosurgical unit (ConMed) with an electrochemically sharpened (1 M NaOH and 120 V) tungsten wire. The tungsten wire was fastened and wound around an extra-fine needle electrode (714, ConMed) to enable current to pass through the sharpened wire. All ablations were performed using 1.5 W of electrical current for 0.5–1 s. During cauterization, larvae were placed on their dorsum on a KimWipe moistened with PBS under a Zeiss Discovery V8 dissection microscope to enable visualization of the leg discs. The left rudimentary wing disc was cauterized using the position of the leg discs and boundaries of the thoracic segments as landmarks. To control for the effect of cauterization and for damage to imaginal tissue, the left posterior leg imaginal disc was cauterized using the same intensity and time of cauterization. After cauterization, larvae were placed in replicates containing adult minor workers to care for them (in a 2:1 adult:larva ratio) until they were either fixed before pupation and DAPI-stained for imaginal disc imaging or left to metamorphose into pupae for pupal imaging and measurements. Analysing the effect of control leg disc ablations on pupae and dissected larvae allowed us to confirm that cauterization was specific to the targeted tissue and did not damage surrounding imaginal tissues (Fig. 2j and Extended Data Fig. 5m–q).

Soldier inhibition and juvenile hormone manipulations. Previous studies have shown that exposure of *Pheidole* larvae to a high density of adult soldiers reduces their potential to develop into soldiers owing to the production of a soldier inhibitory pheromone²³. In particular, bipotential larvae that were treated with a dose of the juvenile hormone analogue methoprene—which would normally induce soldier development—became minor workers when raised by 100% soldiers²⁴. In the absence of adult soldiers, treating size-matched bipotential larvae with methoprene has previously been shown to induce soldier and supersoldier development in *Pheidole* and results in the development of rudimentary wing discs¹⁰. To determine whether the inhibition of soldier development is mediated by rudimentary wing disc growth, sized-matched bipotential larvae were treated with methoprene (5 mg/ml, Sigma-Aldrich) or acetone vehicle control and raised by either 100% minor workers (no inhibition) or 100% soldiers (high inhibition) in a 2:1 adult:larva ratio. Larvae were either fixed before pupation for imaginal disc imaging or left to metamorphose into pupae for pupal imaging and measurements. To determine the effects of this inhibitory pheromone on soldier development, soldier-destined larvae were collected as described in 'RNAi', and placed in replicates that contained 100% adult soldiers (high inhibition) or 100% minor workers (no inhibition) in a 2:1 adult:larva ratio. Larvae were fixed before pupation and DAPI-stained for imaginal disc measurements or left to metamorphose into pupae for pupal imaging and measurements. To determine whether the inhibitory pheromone is involved in regulating head-to-body scaling independent of the disc, bipotential larvae—which do not possess rudimentary discs—were raised with 100% adult soldiers (in a 2:1 adult:larva ratio). These were additionally treated with acetone, to enable comparison to the acetone + 100% minor workers treatment described above. Individual ants were then either fixed as larvae for imaginal disc measurements or left to metamorphose for pupal measurements.

Cuticular hydrocarbon extraction and application. To test whether the soldier inhibitory pheromone is capable of changing head-to-body scaling independent of rearing environment, soldier-destined larvae were treated with cuticular hydrocarbons extracted in a 2:1 adult:larva ratio from adult soldiers. The extraction and application protocol was modified from a previous publication⁵⁵. To extract the surface cuticular hydrocarbons from adult soldiers, adult soldiers were frozen at –80°C for 3 min and then placed in a Teflon-capped borosilicate glass vial (Sigma-Aldrich) containing 50 µl hexane per 10 soldiers for 2 min. Extracts were dried with high-purity nitrogen and resuspended in hexane. Soldier-destined larvae were treated with 1 µl of extract or hexane control and then placed in replicates containing adult minor workers to care for them (in a 2:1 adult:larva ratio). Larvae were left to metamorphose into pupae for pupal imaging and measurements.

Microscopy and morphometrics. Larval and pupal imaging was conducted with a Zeiss Discovery V12 stereomicroscope, while the imaging of imaginal discs

(Bright Field, DIC and fluorescence) was performed with a Zeiss AxioImager Z1 microscope. Larval rudimentary wing discs stained for PH3 were imaged with a confocal Leica SP8 Point-Standing Confocal system on a Leica DMI6000B Inverted Microscope. Zeiss AxioVision software was used to take larval, imaginal disc and pupal measurements. All rudimentary wing disc size measurements were performed on terminal stage larvae just before pupation, as this establishes a standardized stage for comparisons between castes and experimental manipulations⁷. Furthermore, rudimentary wing disc size was compared to leg disc size to normalize for variation among individual ants within the terminal stage. Head width and body length of pupae was measured in a dorsal view because insects obtain their final adult shape and size after they metamorphose, and measurements on pupae are more repeatable and accurate than those on adults.

Statistics and reproducibility. All statistical analyses were performed on Graphpad Prism v.7 and statistical analyses were considered statistically significant at a *P* value < 0.05. All measures were log-transformed before analysis, with the exception of those used to calculate percentage change in head width and body length. To estimate measurement error, 20 wild-type minor worker and 20 wild-type soldier pupae were randomly selected and pupal head width and body length were measured. Each morphological trait was measured three times and the person taking the measures was blind to previous values. A random-effects ANOVA (RStudio, v.1.1.423) was used to estimate the measurement error in log-transformed values for head width and body length. The measurement error was found to make up a negligible percentage of total variance in head width (0.0599%) and body length (0.0822%). Therefore, ordinary least squares linear regression was used throughout because previous work⁵⁶ has shown that the ordinary least squares method is more accurate than reduced major-axis regression when there is low measurement error in the variable on the *x* axis. No statistical methods were used to predetermine sample size, all experiments were independently repeated multiple times and converged on similar results as shown in the Figs. and Extended Data Figs. Blinding and randomization was used during all experimental manipulation.

To test whether any of our manipulations (*vg* RNAi, ablations, high inhibition raised by 100% soldiers, soldier CHC extracts and/or juvenile hormone treatments) altered head-to-body scaling compared to their controls, ANCOVA was used to test for differences in slope and—if no change in slope was observed—differences in *y* intercept between linear regressions of treatment and the respective control were assessed. To compare the ratio of rudimentary wing disc/leg disc area, or the ratio of pupal head width/body length, head width, or body length, normality was first tested using the Shapiro-Wilk test. If normality was violated, a non-parametric Mann-Whitney *U*-test was used, and if not an unpaired *t*-test was used. Where necessary, a Welch's correction for unequal variances was used. All pairwise comparisons were two-tailed except for (1) electrosurgical ablations; (2) percentage change in head width versus body length; and (3) cuticular hydrocarbon treatments, for which we used one-tailed tests based on a priori expectations derived from the results of our preliminary RNAi and soldier inhibition experiments. This workflow was used to determine whether *vg* RNAi, ablations, social and juvenile hormone manipulations, and CHC treatments differed compared to their respective controls for: (1) the ratio of average rudimentary wing disc area to average leg disc area; (2) the ratio of head width to body length; (3) head width; and (4) body length. For multiple pairwise comparisons of head width or body length between social and/or juvenile hormone manipulations and their controls, a Bonferroni correction was applied. Finally, Fisher's exact test was used to determine whether the proportion of males with affected wing morphology differed between *yfp* RNAi control males and *vg* RNAi.

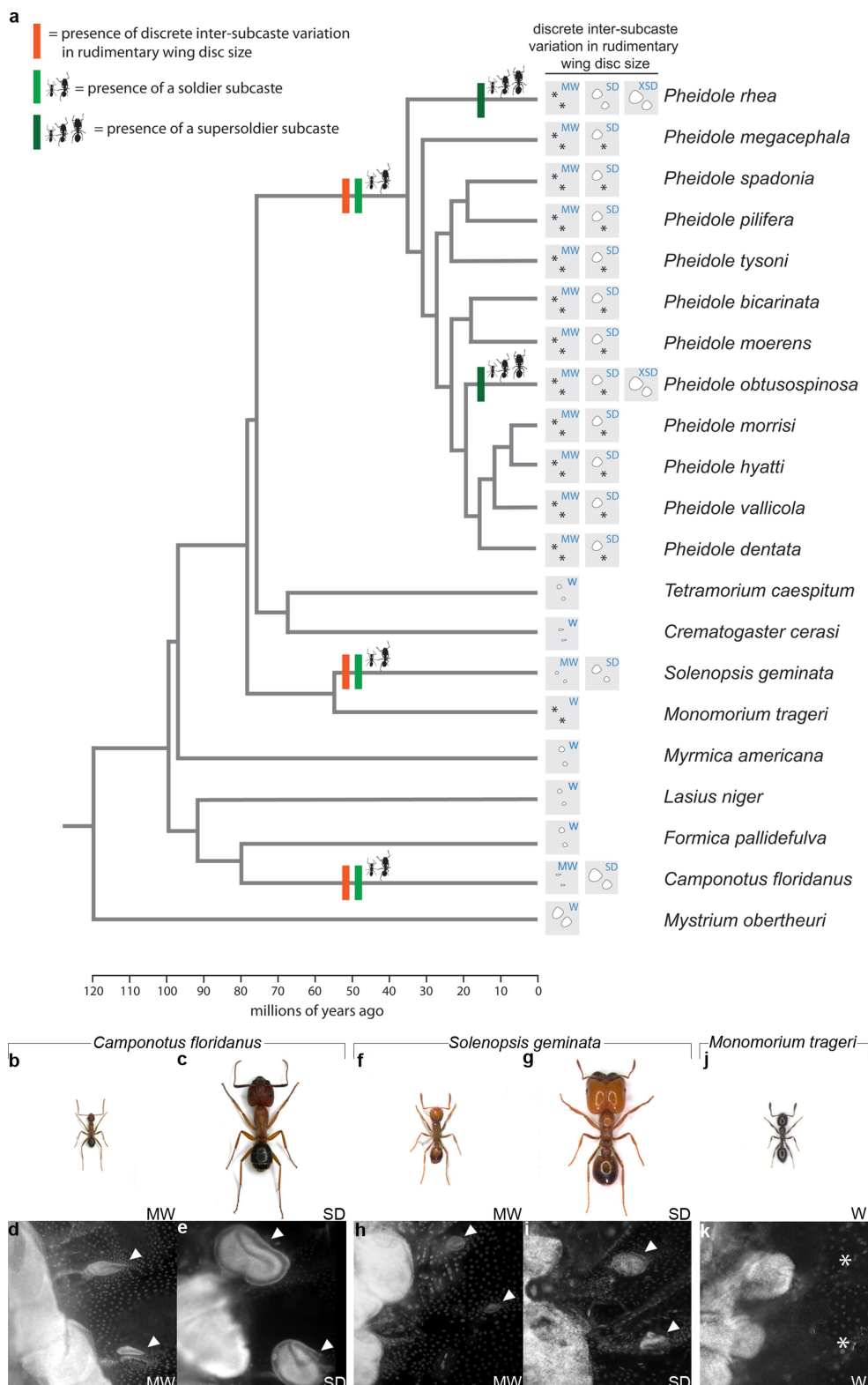
Reporting summary. Further information on research design is available in the Nature Research Reporting Summary linked to this paper.

Data availability

All relevant data are included in the paper. The raw data for all analyses used in this study are available from the corresponding author upon request.

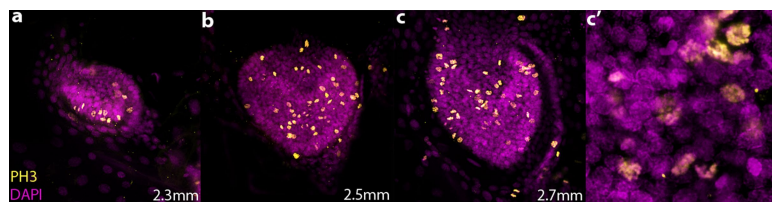
31. Bhatkar, A. & Whitcomb, W. H. Artificial diet for rearing various species of ants. *Fla. Entomol.* **53**, 229–232 (1970).
32. Maddison, W. P. & Maddison, D. R. Mesquite: a modular system for evolutionary analysis. <https://www.mesquiteproject.org/> (2018).
33. Moreau, C. S. & Bell, C. D. Testing the museum versus cradle tropical biological diversity hypothesis: phylogeny, diversification, and ancestral biogeographic range evolution of the ants. *Evolution* **67**, 2240–2257 (2013).
34. Ward, P. S., Brady, S. G., Fisher, B. L. & Schultz, T. R. The evolution of myrmicine ants: phylogeny and biogeography of a hyperdiverse ant clade (Hymenoptera: Formicidae). *Syst. Entomol.* **40**, 61–81 (2015).
35. Ward, P. S. The phylogeny and evolution of ants. *Annu. Rev. Ecol. Evol. Syst.* **45**, 23–43 (2014).
36. Ward, P. S., Blaimer, B. B. & Fisher, B. L. A revised phylogenetic classification of the ant subfamily Formicinae (Hymenoptera: Formicidae), with resurrection of the genera *Colobopsis* and *Dinomyrmex*. *Zootaxa* **4072**, 343–357 (2016).

37. Blaimer, B. B. et al. Phylogenomic methods outperform traditional multi-locus approaches in resolving deep evolutionary history: a case study of formicine ants. *BMC Evol. Biol.* **15**, 271 (2015).
38. Branstetter, M. G. et al. Phylogenomic insights into the evolution of stinging wasps and the origins of ants and bees. *Curr. Biol.* **27**, 1019–1025 (2017).
39. Moreau, C. S. Unraveling the evolutionary history of the hyperdiverse ant genus *Pheidole*. *Mol. Phylogenet. Evol.* **48**, 224–239 (2008).
40. Blanchard, B. D. & Moreau, C. S. Defensive traits exhibit an evolutionary trade-off and drive diversification in ants. *Evolution* **71**, 315–328 (2017).
41. Patel, N. H. Imaging neuronal subsets and other cell types in whole-mount *Drosophila* embryos and larvae using antibody probes. *Methods Cell Biol.* **44**, 445–487 (1994).
42. Khila, A. & Abouheif, E. In situ hybridization on ant ovaries and embryos. *Cold Spring Harb. Protoc.* **2009**, doi:10.1101/pdb.prot5250 (2009).
43. Wheeler, G. C. & Wheeler, J. *Ant Larvae: Review and Synthesis* Memoirs of the Entomological Society of Washington Vol. 7 (The Entomological Society of Washington, Gainesville, 1976).
44. Tautz, D. & Pfeifle, C. A non-radioactive in situ hybridization method for the localization of specific RNAs in *Drosophila* embryos reveals translational control of the segmentation gene hunchback. *Chromosoma* **98**, 81–85 (1989).
45. Lourenço, A. P., Mackert, A., dos Santos Cristina, A. & Simões, Z. L. P. Validation of reference genes for gene expression studies in the honey bee, *Apis mellifera*, by quantitative real-time RT-PCR. *Apidologie (Celle)* **39**, 372–385 (2008).
46. Khila, A., Abouheif, E. & Rowe, L. Function, developmental genetics, and fitness consequences of a sexually antagonistic trait. *Science* **336**, 585–589 (2012).
47. Favé, M. J. et al. Past climate change on Sky Islands drives novelty in a core developmental gene network and its phenotype. *BMC Evol. Biol.* **15**, 183 (2015).
48. Miller, S. C., Miyata, K., Brown, S. J. & Tomoyasu, Y. Dissecting systemic RNA interference in the red flour beetle *Tribolium castaneum*: parameters affecting the efficiency of RNAi. *PLoS ONE* **7**, e47431 (2012).
49. Khila, A., Abouheif, E. & Rowe, L. Evolution of a novel appendage ground plan in water striders is driven by changes in the *Hox* gene *Ultrabithorax*. *PLoS Genet.* **5**, e1000583 (2009).
50. Khila, A., Abouheif, E. & Rowe, L. Comparative functional analyses of ultrabithorax reveal multiple steps and paths to diversification of legs in the adaptive radiation of semi-aquatic insects. *Evolution* **68**, 2159–2170 (2014).
51. Spradling, A. C. & Rubin, G. M. Transposition of cloned P elements into *Drosophila* germ line chromosomes. *Science* **218**, 341–347 (1982).
52. Livramento, K. G. D., Freitas, N. C., Máximo, W. P. F., Zanetti, R. & Paiva, L. V. Gene expression profile analysis is directly affected by the selected reference gene: the case of leaf-cutting *Atta sexdens*. *Insects* **9**, 18 (2018).
53. Shbailat, S. J., Khila, A. & Abouheif, E. Correlations between spatiotemporal changes in gene expression and apoptosis underlie wing polyphenism in the ant *Pheidole morrisii*. *Evol. Dev.* **12**, 580–591 (2010).
54. Nijhout, H. F. Pattern formation on lepidopteran wings: determination of an eyespot. *Dev. Biol.* **80**, 267–274 (1980).
55. Penick, C. A. & Liebig, J. A larval ‘princess pheromone’ identifies future ant queens based on their juvenile hormone content. *Anim. Behav.* **128**, 33–40 (2017).
56. Kilmer, J. T. & Rodríguez, R. L. Ordinary least squares regression is indicated for studies of allometry. *J. Evol. Biol.* **30**, 4–12 (2017).
57. Huang, M. H. & Wheeler, D. E. Colony demographics of rare soldier-polymorphic worker caste systems in *Pheidole* ants (Hymenoptera, Formicidae). *Insect. Soc.* **58**, 539–549 (2011).
58. Shbailat, S. J. & Abouheif, E. The wing-patterning network in the wingless castes of Myrmicine and Formicine ant species is a mix of evolutionarily labile and non-labile genes. *J. Exp. Zool. B Mol. Dev. Evol.* **320**, 74–83 (2013).
59. Bharti, H. & Kumar, R. Taxonomic studies on genus *Tetramorium* Mayr (Hymenoptera, Formicidae) with report of two new species and three new records including a tramp species from India with a revised key. *ZooKeys* **207**, 11–35 (2012).
60. Bolton, B. *Synopsis and Classification of Formicidae* Memoirs of the American Entomological Institute Vol. 71 (American Entomological Institute, Gainesville, 2003).
61. Morgan, C. E. & Mackay, W. *The North America Acrobat Ants of the Hyperdiverse Genus Crematogaster* (Hymenoptera: Formicidae) (Lambert, Saarbrücken, 2017).
62. DuBois, M. B. A revision of the native New World species of the ant genus *Monomorium* (minimum group) (Hymenoptera: Formicidae). *Univ. Kans. Sci. Bull.* **53**, 65–119 (1986).
63. Wilson, E. O. Division of labor in fire ants based on physical castes (Hymenoptera: Formicidae: Solenopsis). *J. Kans. Entomol. Soc.* **51**, 615–636 (1978).
64. Weber, N. A. Description of new North American species and subspecies of *Myrmica* Latreille (Hym.: Formicidae). *Lloydia* **2**, 144–152 (1939).
65. Wilson, E. O. A monographic revision of the ant genus *Lasius*. *Bull. Mus. Comp. Zool.* **113**, 1–204 (1955).
66. Trager, J. C., MacGown, J. A. & Trager, M. D. in *Advances in Ant Systematics (Hymenoptera: Formicidae): Homage to E. O. Wilson — 50 Years Of Contributions* Memoirs of the American Entomological Institute Vol. 80 610–636 (American Entomological Institute, Gainesville, 2007).
67. Béhague, J. et al. Lack of interruption of the gene network underlying wing polyphenism in an early-branching ant genus. *J. Exp. Zool. B Mol. Dev. Evol.* **330**, 109–117 (2018).



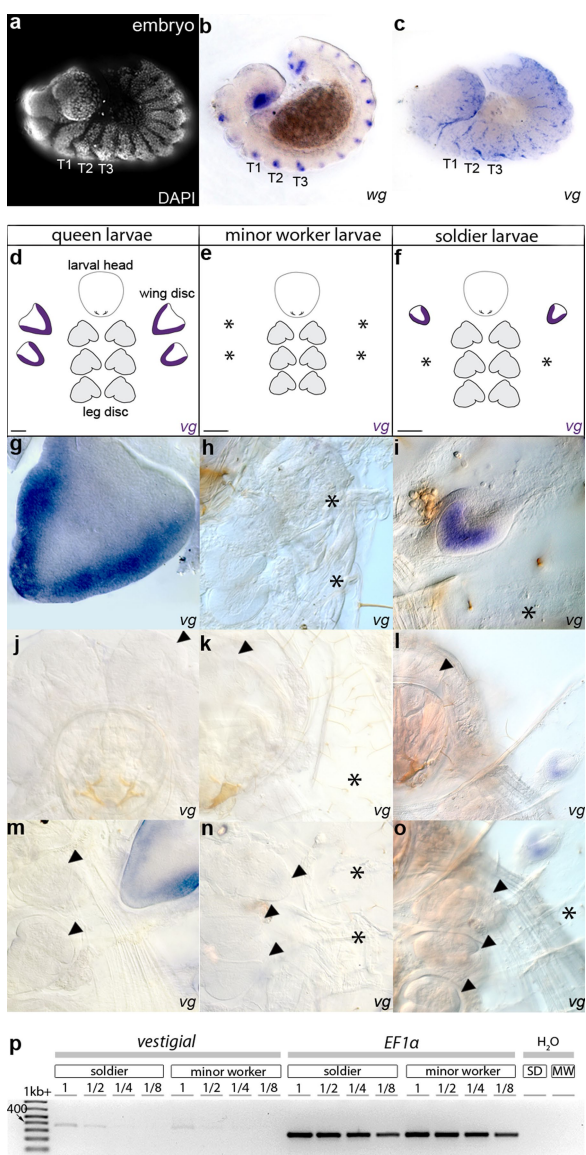
Extended Data Fig. 1 | The phylogenetic correlation between presence of a soldier subcaste and presence of discrete inter-subcaste variation in rudimentary wing disc size. **a**, Pagel's test (difference in log likelihoods = 8.43, $P = 0.001$) shows that there is a significant phylogenetic correlation between the presence of a soldier subcaste and the presence of discrete inter-subcaste variation in the size of rudimentary wing discs, for 21 species of ants. Grey lines indicate phylogenetic relationships, and the time scale of these relationships is indicated at the bottom in millions of years. The orange bar indicates presence of discrete inter-subcaste variation in the size of rudimentary wing discs, the green bar with two adjacent cartoons indicates presence of minor worker and soldier subcastes, and the dark green bar with three adjacent cartoons

indicates presence of minor worker, soldier and supersoldier subcastes. Inter-subcaste variation in the size of rudimentary wing discs in workers (W) and/or minor workers and/or soldiers and/or supersoldiers are at the tip of each branch, where the white-circle drawings represent presence and relative size, within species, of rudimentary wing discs and asterisks indicate absence of rudimentary wing discs. Extended Data Table 1 provides references and descriptions. **b–k**, Adults and rudimentary wing discs of minor workers and/or soldiers and/or workers of *C. floridanus* (**b–e**), *S. geminata* (**f–i**) and *M. trageri* (**j, k**). **d, e, h, i, k**, Arrowheads indicate the presence of rudimentary wing discs and asterisks indicate the absence of rudimentary wing discs. All comparisons within species are to scale.

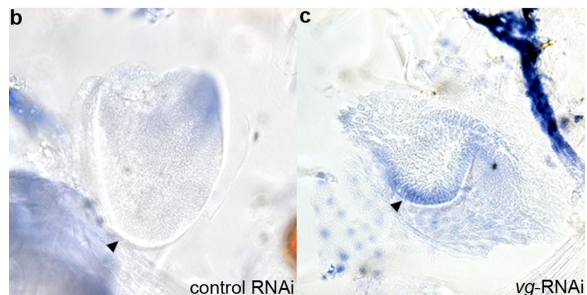
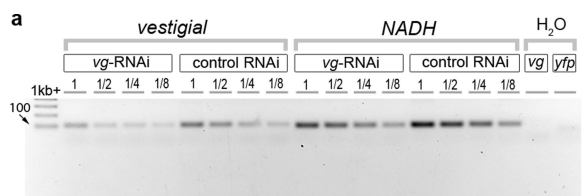


Extended Data Fig. 2 | Proliferation of rudimentary forewing discs in soldier-destined larvae. a–c, Immunohistochemistry of rudimentary forewing discs in *P. hyatti* soldier-destined larvae. DAPI (magenta) stains all nuclei within the cells of rudimentary forewing discs, and phospho-histone H3 (PH3; yellow) stains proliferating cells. The length of the

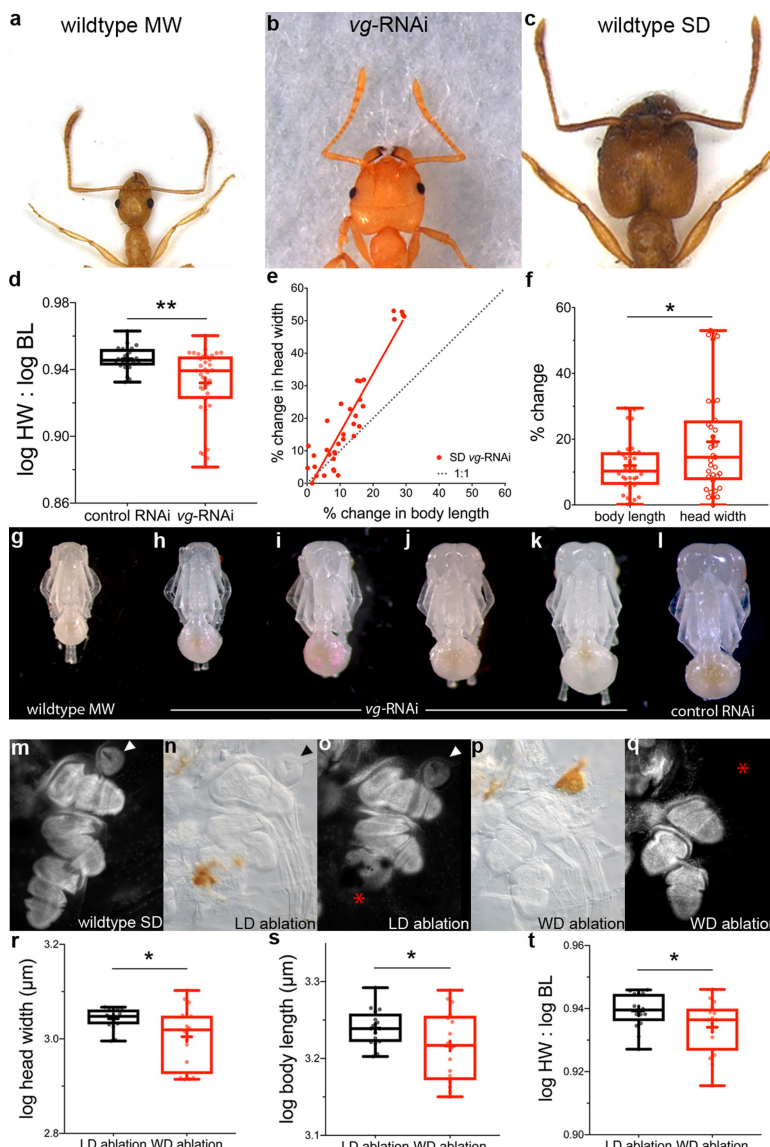
larva from which the rudimentary forewing disc was dissected is given in the bottom right corner. All images are to scale. c' provides an increased magnification of c, to show nuclear co-localization of DAPI and PH3. Experiments were repeated twice.



Extended Data Fig. 3 | Imaginal disc expression of *vg* is restricted to wing discs during larval development in *P. hyatti*. **a–c**, DAPI staining (**a**); *wingless* (*wg*) expression marking segment boundaries (**b**) and *vestigial* (*vg*) expression in the ventral nerve cord and in wing primordial cells in thoracic segments T2 and T3 (**c**) is shown for *P. hyatti* embryos. The three thoracic segments are labelled T1, T2 and T3. Experiments on embryos were repeated twice. **d–f**, Larval cartoons depicting leg discs and wing discs in queens (**d**), leg discs in minor workers (**e**) and leg discs and rudimentary wing discs in soldiers (**f**). Asterisks indicate absence of rudimentary wing discs. *vg* expression is indicated in purple. Lines at bottom right indicate the relative scale. **g–o**, *vg* expression is present in the larval (rudimentary) wing discs and is absent in the head and in leg discs of queens ($n=17$) (**g, j, m**), minor workers ($n=20$) (**h, k, n**) and soldiers ($n=11$) (**i, l, o**). Black arrowheads indicate position of larval head and leg discs, and asterisks indicate absence of rudimentary wing discs. Experiments were repeated at least three times. **p**, Electrophoresis of PCR products obtained using *vg* and *EF1a* primers on wild-type soldier and minor-worker cDNA libraries, each constructed from three terminal-stage larvae. The 1 kb+ ladder is shown as reference and 1, 1/2, 1/4 and 1/8 represent serial dilutions of template cDNA. *vg* transcript (left) is detected in both soldiers and minor workers using semi-quantitative reverse-transcription PCR. The housekeeping *EF1a* transcript (right) is detected in both soldiers and minor workers, and levels are comparable between soldier and minor-worker cDNA libraries across dilutions. Negative controls (water with no template) show no contamination. For uncropped gel source data, see Supplementary Fig. 1. Experiments were repeated with independent biological replicates three times.

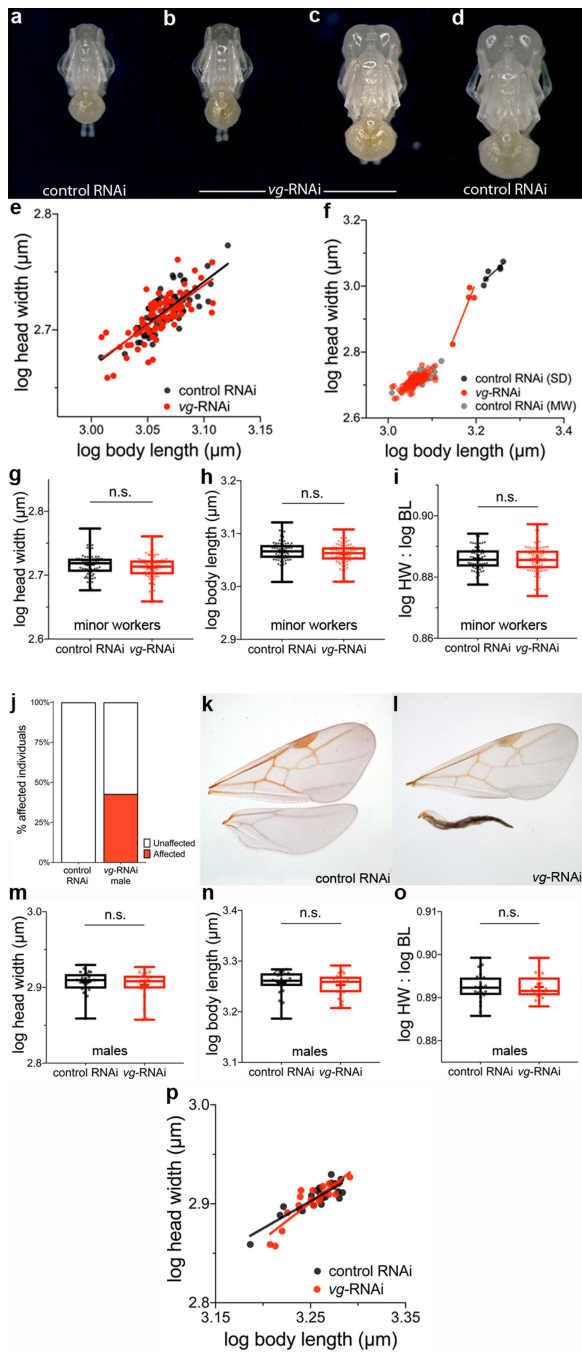


Extended Data Fig. 4 | *vg* RNAi reduces *vg* expression and induces apoptosis in rudimentary forewing discs. **a**, Electrophoresis of PCR products obtained using *vg* and *NADH* primers on soldier cDNA libraries each constructed from three terminal-stage larvae after *vg* RNAi or *yfp* RNAi (control RNAi) injection (Fig. 2a, red arrowhead). The 1 kb+ ladder is shown as reference and 1, 1/2, 1/4 and 1/8 represent serial dilutions of template cDNA. *vg* transcript (left) is detected in both *vg* RNAi and control RNAi libraries using semi-quantitative reverse-transcription PCR. The housekeeping *NADH* transcript (right) is detected in both *vg* RNAi and control RNAi larvae, and levels are comparable between *vg* RNAi and control RNAi cDNA libraries across dilutions. Negative controls (water with no template) show no contamination. Experiments were repeated twice as independent biological replicates. For uncropped gel source data, see Supplementary Fig. 1. **b, c**, Apoptosis revealed by TUNEL assay in rudimentary forewing disc in control RNAi (**b**) and *vg* RNAi (**c**). Compared to control RNAi, *vg* RNAi induces apoptosis along the dorso-ventral margin of rudimentary forewing discs, where wild-type *vg* expression is normally strongest (**b, c**, black arrowhead). Experiments were repeated at least twice.



Extended Data Fig. 5 | Rudimentary forewing discs regulate size and disproportionate head-to-body scaling. **a**, Wild-type adult minor worker. **b**, *vg* RNAi intermediate adult. **c**, Wild-type soldier adult. Images to scale. **d**, Comparing ratios of log(head width (μm)) to log(body length (μm)) (log HW:log BL), between *yfp* RNAi (control RNAi, $n = 23$) and *vg* RNAi ($n = 35$); the box plot shows mean (+), interquartile range (bars), minimum-to-maximum values (whiskers); all points represent individual ants. Two-tailed Mann–Whitney *U*-test, $U = 219$, $**P = 0.0031$. **e**, Percentage change in body length (μm) versus percentage change in head width (μm) of *vg* RNAi compared to a 1:1 line. Each point represents (absolute(HW – HW_{control RNAi average})/HW_{control RNAi average}) × 100 and/or (absolute(BL – BL_{control RNAi average})/BL_{control RNAi average}) × 100. **f**, Comparing the percentage change in body length (μm) and head width (μm) after *vg* RNAi ($n = 35$). The box plot shows mean (+), interquartile range (bars), maximum-to-minimum values (whiskers); all points represent individual ants. One-tailed Mann–Whitney *U*-test, $U = 470$, $*P = 0.0477$. **g**–**l**, Wild-type minor worker. **i**, *yfp* RNAi (control RNAi) soldier. **g**–**l**, *vg* RNAi individuals showing a range of intermediates between minor worker and soldier (see Fig. 2i). Wild-type minor worker is shown for reference in **a**, **g**. All image comparisons are to scale. Experiments

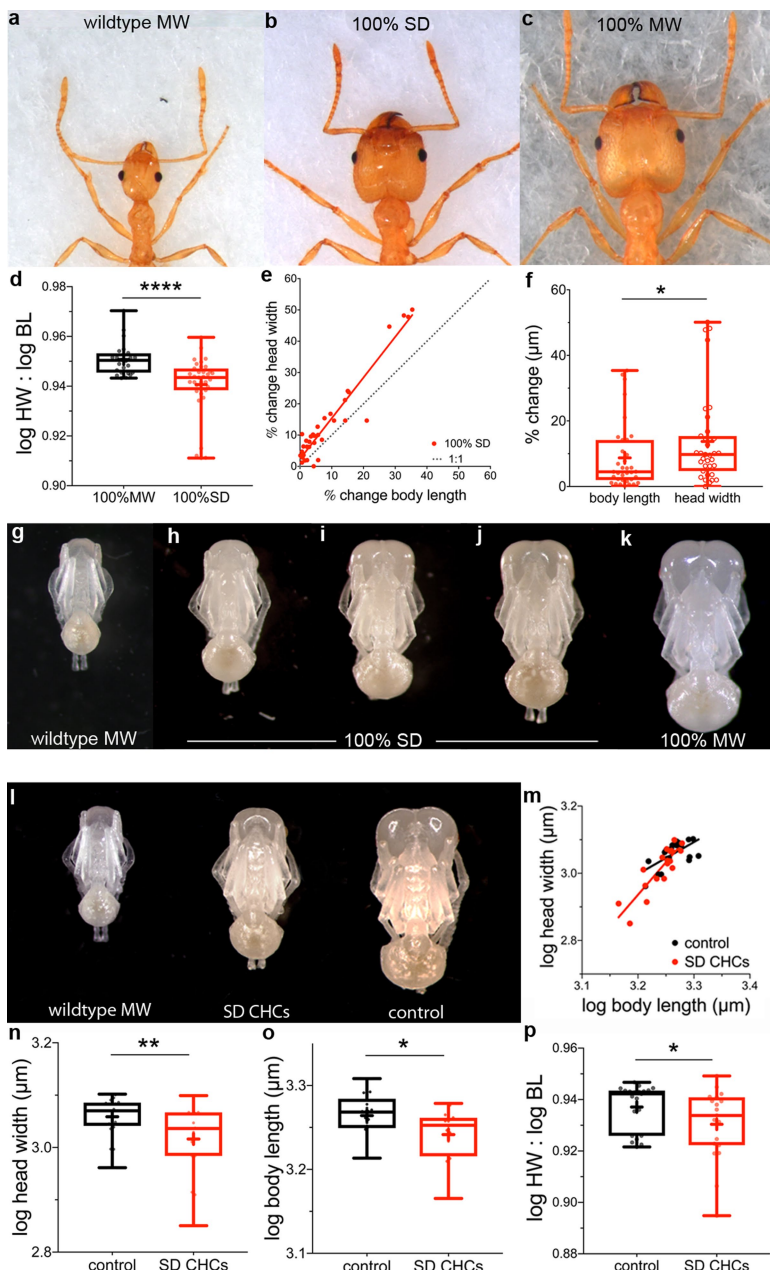
were repeated at least three times. **m**–**t**, Electrosurgical ablation of leg and rudimentary forewing discs in soldier-destined larvae (Fig. 2a, red arrowhead). **m**, Wild-type soldier, leg and rudimentary forewing discs. **n**, Site of leg disc cauterization shown by melanized cuticle. **o**, Ablation of leg disc (DAPI, red asterisk). **p**, Site of rudimentary forewing disc cauterization shown by melanized cuticle. **q**, Ablation of rudimentary forewing disc (DAPI, red asterisk). White or black arrowheads indicate the presence of rudimentary forewing discs. All images are to scale. **r**, Comparing log(head width (μm)) between leg disc ablation ($n = 16$) and rudimentary forewing disc ablation ($n = 16$); one-tailed Mann–Whitney *U*-test, $U = 82$, $*P = 0.0432$. **s**, Comparing log(body length (μm)) between leg disc ablation ($n = 16$) and rudimentary forewing disc ablation ($n = 16$). One-tailed unequal variance *t*-test, $t = 1.77$, d.f. = 22.34, $*P = 0.045$. **t**, Comparing ratio of log(head width (μm)) to log(body length(μm)), between leg disc ablation ($n = 16$) and rudimentary forewing disc ablation ($n = 16$). One-tailed unpaired *t*-test, $t = 2.07$, d.f. = 30, $*P = 0.0234$. The box plots in **d**, **f**, **r**–**t** show mean (+), interquartile range (bars) and minimum-to-maximum values (whiskers); all points represent individual ants. Experiments were repeated at least twice.



Extended Data Fig. 6 | See next page for caption.

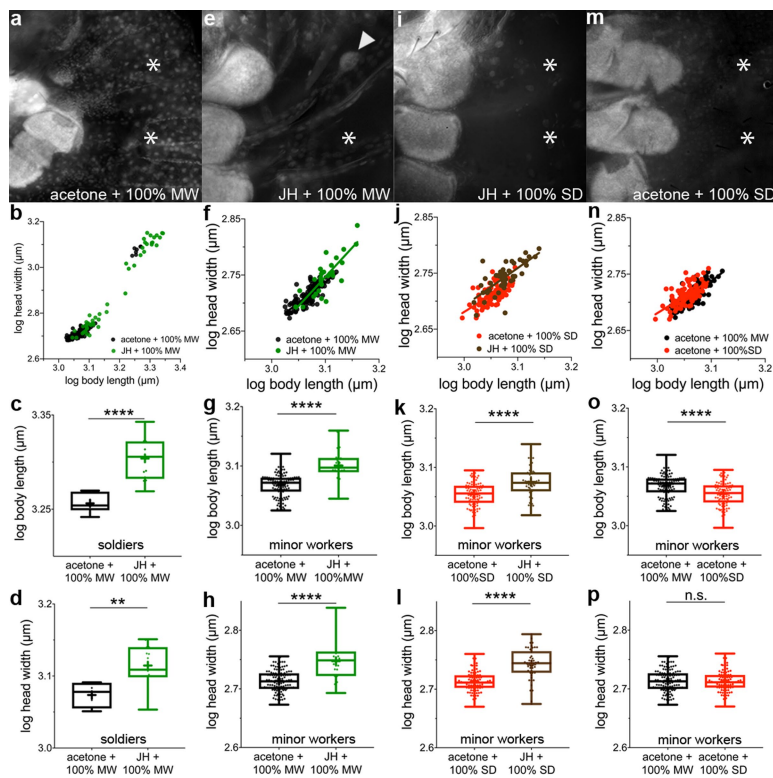
Extended Data Fig. 6 | The function of rudimentary forewing discs in regulating disproportionate head-to-body scaling is specific to the soldier subcaste. *vg* RNAi on bipotential larvae (Fig. 2a, orange arrowhead). **a**, *yfp* RNAi (control RNAi) minor worker. **b**, *vg* RNAi minor worker. **c**, *vg* RNAi intermediate. **d**, *yfp* RNAi (control RNAi) soldier. Image comparisons to scale. **e**, log(body length (μm)) versus log(head width (μm)), comparing minor worker head-to-body scaling of *yfp* RNAi (control RNAi, $n = 69$) and *vg* RNAi ($n = 84$). ANCOVA: slope, $F = 0.162$, d.f. = 149, $P = 0.69$; y intercept, $F = 0.4755$, d.f. = 150, $P = 0.49$. **f**, log(body length (μm)) versus log(head width (μm)), comparing head-to-body scaling of *yfp* RNAi (control RNAi; $n = 6$) and *vg* RNAi ($n = 4$) ants that initiated soldier development. ANCOVA: $F = 7.44$, d.f. = 6, $P = 0.0343$. **g**, Comparing log(head width (μm)) between control RNAi ($n = 69$) and *vg* RNAi ($n = 84$) minor workers. Two-tailed unpaired t -test: $t = 1.62$, d.f. = 151, $P = 0.1074$. **h**, Comparing log(body length (μm)) between control RNAi ($n = 69$) and *vg* RNAi ($n = 84$) minor workers. Two-tailed unpaired t -test: $t = 1.54$, d.f. = 151, $P = 0.1249$. **i**, Comparing ratios of log(head width (μm)) to log(body length (μm)) between control RNAi ($n = 69$) and *vg* RNAi ($n = 84$) minor workers. Two-tailed

unpaired t -test: $t = 0.26$, d.f. = 151, $P = 0.80$. Experiments were repeated at least three times. **j–p**, *vg* RNAi on male-destined larvae (Fig. 2a, green arrowhead). **j**, Bar graph showing percentage of individual ants affected (red) after *yfp* RNAi (control RNAi; $n = 0$ out of 23) and *vg* RNAi ($n = 9$ out of 21). Two-tailed Fisher's exact test: $P = 0.0004$. **k, l**, Wings from *yfp* RNAi (control RNAi) (**k**) and *vg* RNAi (**l**) males. Image comparisons are to scale. **m–o**, Head-to-body scaling of *yfp* RNAi (control RNAi; $n = 23$) and *vg* RNAi males ($n = 21$), comparing log(head width (μm)), two-tailed Mann–Whitney U -test, $U = 222.5$, $P = 0.6626$ (**m**); log(body length (μm)), two-tailed Mann–Whitney U -test, $U = 198$, $P = 0.3157$ (**n**); and ratio of log(head width (μm)) to log(body length (μm)) (**o**), between control RNAi males and *vg* RNAi males, two-tailed unpaired t -test, $t = 0.18$, d.f. = 42, $P = 0.86$. **p**, log(body length (μm)) versus log(head width (μm)) comparison of head-to-body scaling, between *yfp* RNAi (control RNAi; $n = 23$) and *vg* RNAi males ($n = 21$). ANCOVA: slope, $F = 3.111$, d.f. = 40, $P = 0.0854$; y intercept, $F = 0.076$, d.f. = 41, $P = 0.7837$. Experiments were repeated at least three times. The box plots in **g–i** and **m–o** show mean (+), interquartile range (bars) and minimum-to-maximum values (whiskers); all points represent individual ants.



Extended Data Fig. 7 | Soldier inhibitory pheromone regulates size and disproportionate head-to-body scaling. **a–k**, Effect of social inhibition on soldier-destined larvae (Fig. 2a, red arrowhead). **a**, Wild-type adult minor worker. **b**, Intermediate adult resulting from soldier-destined larvae being raised in colonies composed of 100% soldiers (high inhibition). **c**, Representative adult soldier resulting from soldier-destined larvae being raised in colonies composed of 100% minor workers (no inhibition). **d**, Comparing ratios of $\log(\text{head width} \text{ } (\mu\text{m}))$ to $\log(\text{body length} \text{ } (\mu\text{m}))$ between 100% minor worker ($n = 24$) and 100% soldier ($n = 35$). The box plot shows mean (+), interquartile range (bars) and minimum-to-maximum values (whiskers); all points represent individual ants. Two-tailed Mann–Whitney U -test, $U = 155$, $***P < 0.0001$. **e**, Percentage change in body length (μm) versus percentage change in head width (μm) of 100% soldiers, compared to a 1:1 line. Each point represents $(\text{absolute}(\text{HW} - \text{HW}_{\text{100\% minor worker average}})/\text{HW}_{\text{100\% minor worker average}}) \times 100$ and/or $(\text{absolute}(\text{BL} - \text{BL}_{\text{100\% minor worker average}})/\text{BL}_{\text{100\% minor worker average}}) \times 100$. **f**, Comparing percentage change in body length (μm) and head

width (μm) following high inhibition (100% soldiers; $n = 35$). One-tailed Mann–Whitney U -test, $U = 421$, $*P = 0.0121$. **g**, Wild-type minor worker. **h–j**, 100% soldier-raised ants showing a range of intermediates between minor workers and soldiers (see Fig. 3e). **k**, 100% minor-worker control soldier. All image comparisons are to scale. Experiments were repeated at least three times. **l–p**, Application of soldier cuticular hydrocarbon extract (CHCs) to soldier-destined larvae (Fig. 2a, red arrowhead). **l**, Wild-type minor worker and individual ants treated with soldier CHCs and hexane solvent (control). **m**, Comparing slopes of hexane solvent control ($n = 21$) and soldier CHCs ($n = 19$). ANCOVA, $F = 6.84$, d.f. = 36, $P = 0.0129$. **n**, $\log(\text{head width} \text{ } (\mu\text{m}))$; one-tailed Mann–Whitney U -test, $U = 114$, $**P = 0.0099$. **o**, $\log(\text{body length} \text{ } (\mu\text{m}))$; one-tailed Mann–Whitney U -test, $U = 117$, $*P = 0.0126$. **p**, Ratio of $\log(\text{head width} \text{ } (\mu\text{m}))$ to $\log(\text{body length} \text{ } (\mu\text{m}))$; one-tailed Mann–Whitney U -test, $U = 125$, $*P = 0.0221$. Wild-type minor worker is shown for reference in **a**, **g**, **l**. The box plots in **d**, **f**, **n–p** show mean (+), interquartile range (bars), minimum-to-maximum values (whiskers); all points represent individual ants.



Extended Data Fig. 8 | Juvenile hormone and inhibitory pheromone regulate disc-dependent disproportionate head-to-body scaling and disc-independent proportional head:body scaling. Effect of juvenile-hormone activation and social inhibition on bipotential larvae (Fig. 2a, orange arrowhead). **a**, Absence of rudimentary wing discs in minor worker larvae exposed to solvent control with no inhibition ('acetone + 100% MW'). **a, e, i, m**, Arrowheads indicate the presence of rudimentary wing discs and asterisks indicate the absence of rudimentary wing discs. **b**, Plot of head-to-body scaling of acetone + 100% minor worker, and juvenile-hormone activation with no inhibition ('JH + 100% MW'); the majority of larvae treated with juvenile hormone develop into soldiers, and some develop into large minor workers. **c, d**, Comparing between acetone + 100% minor worker ($n=7$) and juvenile hormone + 100% minor worker ($n=17$) treatments of individuals that developed into the soldier size distribution. **c**, $\log(\text{body length} \text{ } (\mu\text{m}))$; two-tailed unpaired t -test; $t = 5.25$, $d.f. = 22$, $****P < 0.0001$. **d**, $\log(\text{head width} \text{ } (\mu\text{m}))$; two-tailed unpaired t -test, $t = 3.50$, $d.f. = 22$, $**P = 0.002$. **e**, Initiation of growth of rudimentary forewing discs in minor worker larvae exposed to juvenile hormone + 100% minor worker. **f**, Plot of head-to-body scaling between acetone + 100% minor worker ($n=114$) and juvenile hormone + 100% minor worker ($n=29$) of individuals that developed into the minor-worker size distribution. ANCOVA: $F = 7.12$, $d.f. = 139$, $P = 0.0085$. **g, h**, Comparing between acetone + 100% minor worker ($n=114$) and juvenile hormone + 100% minor worker ($n=29$) treatments of individuals that developed into the minor-worker size distribution. **g**, $\log(\text{body length} \text{ } (\mu\text{m}))$; two-tailed Mann–Whitney U -test, $U = 463$, $****P < 0.0001$. **h**, $\log(\text{head width} \text{ } (\mu\text{m}))$; two-tailed unequal variance t -test, $t = 5.19$, $d.f. = 32$, $****P < 0.0001$. **i**, Absence of growth of rudimentary wing discs in minor worker larvae exposed to juvenile-

hormone activation with high inhibition ('JH + 100% SD'). **j**, Plot of head-to-body scaling between solvent control with high inhibition ('acetone + 100% SD'; $n=88$) and juvenile hormone + 100% soldiers ($n=46$) of individuals that developed into the minor-worker size distribution. ANCOVA: slope, $F = 0.54$, $d.f. = 130$, $P = 0.47$; y intercept, $F = 27.2$, $d.f. = 131$, $P < 0.0001$. **k, l**, Comparing between acetone + 100% soldiers ($n=88$) and juvenile hormone + 100% soldiers ($n=46$) treatments of individuals that developed into the minor-worker size distribution. **k**, $\log(\text{body length} \text{ } (\mu\text{m}))$; two-tailed unequal variance t -test, $t = 4.43$, $d.f. = 69$, $****P < 0.0001$. **l**, $\log(\text{head width} \text{ } (\mu\text{m}))$; two-tailed unequal variance t -test, $t = 6.69$, $d.f. = 68$, $****P < 0.0001$. **m**, Absence of rudimentary wing disc growth in minor worker larvae exposed to acetone + 100% soldiers. **n**, Plot of head-to-body scaling between acetone + 100% minor workers ($n=114$) and acetone + 100% soldiers ($n=88$) treatments of individuals that developed into the minor-worker size distribution. ANCOVA: slope, $F = 2.84$, $d.f. = 198$, $P = 0.0937$; y intercept, $F = 20.77$, $d.f. = 199$, $P < 0.0001$. **o, p**, Comparing between acetone + 100% minor workers ($n=114$) and acetone + 100% soldiers ($n=88$) treatments of individuals that developed into the minor-worker size distribution. **o**, $\log(\text{body length} \text{ } (\mu\text{m}))$; two-tailed Mann–Whitney U -test, $U = 3178$, $****P < 0.0001$. **p**, $\log(\text{head width} \text{ } (\mu\text{m}))$; two-tailed unpaired t -test, $t = 0.28$, $d.f. = 200$, $P = 0.7823$. Bonferroni correction was applied to comparison of $\log(\text{head width})$ and $\log(\text{body length})$. The box plots in **c, d, g, h, k, l, o, p** show mean (+), interquartile range (bars) and minimum-to-maximum values (whiskers); all points represent individual ants. Plots in **b, f, j, n** show linear regressions in which the x axis is $\log(\text{body length} \text{ } (\mu\text{m}))$ and the y axis is $\log(\text{head width} \text{ } (\mu\text{m}))$. All images are to scale. Experiments were repeated at least three times.

Extended Data Table 1 | Description and references for presence or absence of soldier subcaste and discrete variation in rudimentary wing disc size across 21 ant species

Species	Presence of a soldier (major worker) subcaste	Reference	Inter-subcaste variation in rudimentary wing disc size?	Description of variation in rudimentary wing disc size	Reference
<i>Pheidole rhea</i>	Yes	Wilson ⁸ , Rajakumar et al. ¹⁰ , Huang & Wheeler ⁵⁷	Yes	MW= no visible discs SD = 2 pairs of discs XSD = 2 pairs of large discs	Rajakumar et al. ¹⁰
<i>Pheidole megacephala</i>	Yes	Wilson ⁸	Yes	MW= no visible discs SD = 1 pair of forewing discs	Rajakumar et al. ¹⁰ , Sameshima et al. ¹¹
<i>Pheidole spadonia</i>	Yes	Wilson ⁸ , Huang & Wheeler ⁵⁷	Yes	MW= no visible discs SD = 1 pair of forewing discs	Rajakumar et al. ¹⁰
<i>Pheidole pilifera</i>	Yes	Wilson ⁸	Yes	MW= no visible discs SD = 1 pair of forewing discs	Rajakumar et al. ¹⁰
<i>Pheidole tysoni</i>	Yes	Wilson ⁸	Yes	MW= no visible discs SD = 1 pair of forewing discs	Rajakumar et al. ¹⁰
<i>Pheidole bicarinata</i>	Yes	Wilson ⁸ , Wheeler & Nijhout ⁹	Yes	MW= no visible discs SD = 1 pair of forewing discs	Wheeler & Nijhout ⁹
<i>Pheidole moerens</i>	Yes	Wilson ⁸	Yes	MW= no visible discs SD = 1 pair of forewing discs	Rajakumar et al. ¹⁰
<i>Pheidole obtusospinosa</i>	Yes	Wilson ⁸ , Rajakumar et al. ¹⁰ , Huang & Wheeler ⁵⁷	Yes	MW= no visible discs SD = 1 pairs of forewing discs XSD = 2 pairs of large discs	Rajakumar et al. ¹⁰ , Present study
<i>Pheidole morrisi</i>	Yes	Wilson ⁸	Yes	MW= no visible discs SD = 1 pair of forewing discs	Abouheif & Wray ⁷ , Rajakumar et al. ¹⁰ , Shbailat & Abouheif ⁵⁸
<i>Pheidole hyatti</i>	Yes	Wilson ⁸	Yes	MW= no visible discs SD = 1 pair of forewing discs	Rajakumar et al. ¹⁰ , Present study
<i>Pheidole vallicola</i>	Yes	Wilson ⁸	Yes	MW= no visible discs SD = 1 pair of forewing discs	Rajakumar et al. ¹⁰
<i>Pheidole dentata</i>	Yes	Wilson ⁸	Yes	MW= no visible discs SD = 1 pair of forewing discs	Rajakumar et al. ¹⁰
<i>Tetramorium caespitum</i>	No	Bharti & Kumar ⁵⁹ , Bolton ⁶⁰	No	W = 2 pairs of small wing discs	Shbailat & Abouheif ⁵⁸
<i>Crematogaster cerasi</i>	No	Morgan & Mackay ⁶¹	No	W = 2 pairs of small wing pads	Abouheif & Wray ⁷ , Shbailat & Abouheif ⁵⁸
<i>Monomorium trageri</i>	No	Dubois ⁶²	No	W = no visible discs	Present study
<i>Solenopsis geminata</i>	Yes	Tschinkel ³⁰ , Wilson ⁶³	Yes	MW = 2 pairs of small wing pads SD = 2 pairs of large wing discs	Present study
<i>Myrmica americana</i>	No	Weber ⁶⁴	No	W = 2 pairs of small wing discs	Abouheif & Wray ⁷
<i>Lasius niger</i>	No	Wilson ⁶⁵	No	W = 2 pairs of small wing discs	Shbailat & Abouheif ⁵⁸
<i>Formica pallidefulva</i> (described as <i>Neoformica nitidiventris</i> in ⁷)	No	Trager, MacGown & Trager ⁶⁶	No	W = 2 pairs of small wing discs	Abouheif & Wray ⁷
<i>Camponotus floridanus</i>	Yes	Alvarado ²⁹ , Wilson ³	Yes	MW = 2 pairs of small wing pads SD = 2 pairs of large wing discs	Present study
<i>Mysterium obertheuri</i>	No	Béhague et al. ⁶⁷	No	W = 2 pairs of wing discs	Béhague et al. ⁶⁷

MW, minor worker; SD, soldier; W, worker; XSD, supersoldier. Refer to Extended Data Fig. 1a for the phylogeny. Data were obtained from previous publications^{7–11,57–67}.

Reporting Summary

Nature Research wishes to improve the reproducibility of the work that we publish. This form provides structure for consistency and transparency in reporting. For further information on Nature Research policies, see [Authors & Referees](#) and the [Editorial Policy Checklist](#).

Statistical parameters

When statistical analyses are reported, confirm that the following items are present in the relevant location (e.g. figure legend, table legend, main text, or Methods section).

n/a Confirmed

- The exact sample size (n) for each experimental group/condition, given as a discrete number and unit of measurement
- An indication of whether measurements were taken from distinct samples or whether the same sample was measured repeatedly
- The statistical test(s) used AND whether they are one- or two-sided
Only common tests should be described solely by name; describe more complex techniques in the Methods section.
- A description of all covariates tested
- A description of any assumptions or corrections, such as tests of normality and adjustment for multiple comparisons
- A full description of the statistics including central tendency (e.g. means) or other basic estimates (e.g. regression coefficient) AND variation (e.g. standard deviation) or associated estimates of uncertainty (e.g. confidence intervals)
- For null hypothesis testing, the test statistic (e.g. F , t , r) with confidence intervals, effect sizes, degrees of freedom and P value noted
Give P values as exact values whenever suitable.
- For Bayesian analysis, information on the choice of priors and Markov chain Monte Carlo settings
- For hierarchical and complex designs, identification of the appropriate level for tests and full reporting of outcomes
- Estimates of effect sizes (e.g. Cohen's d , Pearson's r), indicating how they were calculated
- Clearly defined error bars
State explicitly what error bars represent (e.g. SD, SE, CI)

Our web collection on [statistics for biologists](#) may be useful.

Software and code

Policy information about [availability of computer code](#)

Data collection

All measurements of pupae and larval rudimentary wing discs were performed using Zeiss AxioVision v4.9.1.

Data analysis

Phylogenetic analyses were performed on Mesquite v3.5. Amino acid alignments were performed on Geneious (R8). All statistical analyses were performed using Prism GraphPad v7, except for a random effects ANOVA which was performed on RStudio (Version 1.1.423).

For manuscripts utilizing custom algorithms or software that are central to the research but not yet described in published literature, software must be made available to editors/reviewers upon request. We strongly encourage code deposition in a community repository (e.g. GitHub). See the Nature Research [guidelines for submitting code & software](#) for further information.

Data

Policy information about [availability of data](#)

All manuscripts must include a [data availability statement](#). This statement should provide the following information, where applicable:

- Accession codes, unique identifiers, or web links for publicly available datasets
- A list of figures that have associated raw data
- A description of any restrictions on data availability

All relevant data have been included in the paper. The raw data for all analyses used in this study are available from the corresponding author upon request.

Field-specific reporting

Please select the best fit for your research. If you are not sure, read the appropriate sections before making your selection.

Life sciences

Behavioural & social sciences

Ecological, evolutionary & environmental sciences

For a reference copy of the document with all sections, see nature.com/authors/policies/ReportingSummary-flat.pdf

Life sciences study design

All studies must disclose on these points even when the disclosure is negative.

Sample size

- (1) For *in situ* hybridization, we considered sample sizes sufficient when we could reliably observe consistent expression patterns across castes and between tissues of each caste across multiple runs. Our sample sizes are conservative and higher than previous studies on ant development for confirming presence or absence of gene expression.
- (2) Our ability, for example, to detect a significant difference between controls and experimental treatments at a significance level of alpha = 0.05, even after Bonferroni correction on statistical tests in Extended Data Figure 8g,h,k,l,o,p, suggest that samples sizes were sufficient to limit type 1 errors. For Extended Data Fig. 6j-p, sample sizes provided sufficient statistical power to detect a significant difference in wing patterning defects between vg RNAi treated male-destined larvae and control male-destined larvae. These phenotypic wing defects are also consistent with initial runs. No significant difference was detected between vg-RNAi and control individuals for the ratio of head width:body size or their slope or intercept. While we did not perform a statistical method to predetermine sample size, for these experiments our sample sizes for all manipulations (including dsRNA injection, ablations, hormonal, social and soldier cuticular hydrocarbon extract manipulations) are reasonably high, conservative and consistent with that in previous studies using these techniques in insects. We therefore considered the risk of type 2 error to be low.
- (3) While an equal number of samples were initially allocated for each treatment, the final sample sizes are subject to mortality rate amongst each treatment.

Data exclusions

- For *in situ* hybridization, immunohistochemistry, measurements of imaginal discs and measurements of pupae, we pre-established a set of criteria for removing any samples that were damaged during the experimental run or while handling post-experiment. We excluded any individuals that were damaged or malformed to ensure all morphometric landmarks and tissues were observable to allow consistent measurement acquisition process. Data exclusion was blinded to treatment and applied across all controls and treatments.

Replication

- (1) Results of the RNAi (dsRNA) injection, ablations, social manipulation, soldier extract applications and hormonal treatments are consistent with findings from our initial runs.
- (2) Results of the RNAi (dsRNA) injection, ablations, social manipulation, soldier cuticular hydrocarbon extract applications and hormonal treatments are consistent across experiments. For example, our results from Extended Data Figure 6f (vg RNAi on bipotential larvae that develop into soldiers) are consistent with our results from Fig. 2 and Extended Data Fig. 5 (vg-RNAi on soldier-destined larvae) and our results from electrosurgical ablation of the left rudimentary forewing disc are consistent with results from vg-RNAi in soldier-destined larvae (Fig. 2 and Extended Data Fig. 5).
- (3) RNAi (dsRNA) injection, ablations, social manipulation, soldier extract applications, and hormonal experiments were set up and performed in multiple independent replicates. Each experiment was performed at least twice. Maintenance of developing individuals post-treatment was similar: all replicate colonies were allocated the exact same amount of food at the same frequency (i.e.: everyday). Our results were consistent across multiple replicates and were pooled for statistical analysis.
- (4) Our parameters and results for social manipulation and hormonal treatments are consistent with previous results from another *Pheidole* species, (Wheeler & Nijhout, 1981, 1983; Wheeler and Nijhout 1984) and we show that application of soldier hydrocarbon extracts on soldier-destined larvae is consistent with raising larvae with 100% soldiers (Fig. 3 and Extended Data Fig. 7).
- (5) *In situ* hybridization and immunohistochemistry experiments were replicated several times independently for all castes/specimen types.
- (6) Semi-quantitative PCR was replicated independently several times. All above-mentioned experiments were conducted with appropriate controls described in the manuscript.

Randomization

- For all injection, ablations, social manipulation, soldier cuticular hydrocarbon extract and hormonal treatments, larvae were first selected by size categories and then equally divided to account for number of replicates (including both treatments and controls) before replicate colonies were setup. That is, we did not know what an individual was going to be treated with at the time of their randomized selection. The only thing that was absolutely controlled for was that for all treatments individuals were equally allocated such that they represent the same size and developmental range between treatment and respective controls. Adult ants selected to nurse all treated developing individuals were also selected randomly without pre-knowledge of the treatment group they were going to be included in. For *in situ* hybridization and immunohistochemistry experiments, all larvae were selected randomly from the colony and filtered based on whether they were within the appropriate size and developmental stage range.

Blinding

- For experimental manipulations, different individuals were responsible for different aspects of the experimental runs and analyses for the following steps: sample collection from colonies, sample filtering based on size and developmental staging for treatment, treatment of samples, replicate feeding and maintenance, and data acquisition and analysis. For any given experimental comparison, these steps were conducted such that individuals did not communicate the results or sample identity that were used in subsequent steps.

Reporting for specific materials, systems and methods

Materials & experimental systems

n/a	Involved in the study
<input checked="" type="checkbox"/>	Unique biological materials
<input type="checkbox"/>	Antibodies
<input checked="" type="checkbox"/>	Eukaryotic cell lines
<input checked="" type="checkbox"/>	Palaeontology
<input type="checkbox"/>	Animals and other organisms
<input checked="" type="checkbox"/>	Human research participants

Methods

n/a	Involved in the study
<input checked="" type="checkbox"/>	ChIP-seq
<input checked="" type="checkbox"/>	Flow cytometry
<input checked="" type="checkbox"/>	MRI-based neuroimaging

Antibodies

Antibodies used

Mouse monoclonal anti-PH3 (PH3 Ser10, Cell Signaling Technology 9706S), secondary antibody, goat anti-mouse Alexa 555 (AbCam, AB150114), digoxigenin-labelled riboprobe (Roche Diagnostics Canada).

Validation

Mouse monoclonal anti-PH3 (PH3 Ser10, Cell Signaling Technology 9706S), primary antibody was used at a 1:25 dilution and the secondary antibody, goat anti-mouse Alexa 555 (AbCam, AB150114) was used at a 1:500 dilution. This PH3 antibody was used previously in ants (Fave, M.J. et al. 2015) and shows cross-reactivity in several species, including *Drosophila* (Grillo-Hill, B.K. et al. 2015), mouse (Anderson, M.J. et al. 2016; Bai, L. et al. 2015), and zebrafish (Shin, J. et al. 2012). A digoxigenin-labelled riboprobe (Roche Diagnostics Canada) for vestigial was synthesized from the cloned *Pheidole hyatti* vestigial fragment and an anti-DIG-alkaline phosphatase secondary antibody was used to detect probe expression pattern. This secondary antibody has been used to detect digoxigenin-labelled riboprobes in several different ant species (Abouheif & Wray, Science, 2002; Rajakumar et al., Science, 2012).

Animals and other organisms

Policy information about [studies involving animals](#); [ARRIVE guidelines](#) recommended for reporting animal research

Laboratory animals

Did not involve laboratory animals.

Wild animals

Mature colonies of *Pheidole hyatti* and *Pheidole obtusospinosa* were collected in southwest Arizona, US. Single mated queens of *Camponotus floridanus* and *Monomorium trageri*, and larvae of *Solenopsis geminata* were collected in Florida, US.

Field-collected samples

Colonies of *Pheidole hyatti* and *Pheidole obtusospinosa* were collected in the southwest of Arizona, USA. *Camponotus floridanus* colonies were collected as newly mated queens in Tallahassee, Florida, USA. *Monomorium trageri* colonies and *Solenopsis geminata* larvae were collected in Gainesville, Florida, USA. All colonies and experimental replicates were kept at 27°C with 60% humidity and a 12:12 hour light:dark cycle. They were kept in fluor-coated plastic boxes with cotton-constrained glass water tubes as well as sugar water tubes. They were fed mealworms and Bhatkar-Whitcomb diet. Holes were inserted in the lids of the boxes and lined with mesh to allow better air exchange.